Cyclic Load Resistance of Reinforced Concrete Beams Retrofitted with Composite Laminates

by

Eugene Chuang

B.S. in Civil Engineering, M.I.T. 1996

Submitted to the Department of Civil and Environmental Engineering
in partial fulfillment of the requirements for the degree of
Master of Science
in Civil and Environmental Engineering

Massachusetts Institute of Technology

May 1998

Signature of Author_____
Department of Civil and Environmental Engineering
March 22, 1998

Certified by_____
Oral Buyukozturk
Professor of Civil and Environmental Engineering
Thesis Supervisor

Accepted by_____
Professor Joseph M. Sussman
Chairman, Departmental Graduate Committee

Cyclic Load Resistance of Reinforced Concrete Beams Retrofitted with Composite Laminates

by

Eugene Chuang

Submitted to the Department of Civil and Environmental Engineering
on May 22, 1998, in partial fulfillment of the
requirements for the degree of
Master of Science in Civil and Environmental Engineering

Abstract

This thesis deals with the experimental study of cyclic load resistance of reinforced concrete (RC) beams retrofitted with composite laminates. Using a fracture mechanics approach, the fatigue resistance of the concrete-laminate bond is examined. Three-foot long retrofitted RC beams, scaled down versions of specimens used in antecedent research, were tested. Variables of the experimental program were surface preparation techniques and laminate types. Initial delaminations (in the concrete layer directly above the laminate) were artificially manufactured. The concrete-laminate interfacial region was investigated using a two-part experimental program: static load testing and cyclic load testing.

Static load tests were performed on laminated beams with initial delaminations. All these beams had failures of the concrete-laminate interface which initially propagated along the interface through the concrete. Thus the fracture properties of the concrete was shown to be a significant factor in the peel-off failure of retrofitted beams. The static load tests were used to construct failure interaction curves which revealed the influence of FRP stiffness, delamination location, and concrete surface preparation on the system's delamination resistance.

The cyclic load tests provided fatigue curves which plotted the delamination growth rate against the ratio of cyclic load range to delamination load. Delamination propagation occurred at cyclic load ranges lower than the static strength of this concrete-laminate interface, showing the susceptibility of this interface to fatigue loading. From the fatigue curves Paris Power Law constants were estimated and compared to known Paris Power Law constants. It was revealed that at high-intensity load levels the interfacial fatigue resistance is relatively insensitive to changes in stress intensity; however, the crack propagation rate is usually severe. Thus the interface is vulnerable to long-term, high-intensity loading. Additionally, both the static and cyclic results suggest that the delaminations, which are manifested as concrete cracks, are probably propagating under mode II or mixed mode conditions.

The static and cyclic load test results obtained in this research program yielded a deeper understanding of the behavior of the delamination resistance of the concrete-laminate interface. This understanding creates suggestions for improvements in the use of this post-reinforcement technology, as well as guidelines for the use and design of post-reinforcement. Finally, ideas for further research are proposed.

Thesis Supervisor: Oral Buyukozturk
Title: Professor, Department of Civil and Environmental Engineering

Acknowledgements

I would like to thank the administration and faculty at MIT who supported and helped me with my research, notably Dr. Germaine, Prof. McGarry, and Prof. Wooh.

I express gratitude to the Sika cooperation, especially Joe Mockapetris, for its charitable donation of materials.

I would also like to thank my undergraduate research assistants for their devotion to this project: Rocky Bryant, Mark Audigier, Ashok Eastman, and Alan Chhabra.

I want to thank my office mates, particularly Brian Hearing, for their generous input and guidance.

A special thanks goes to Prof. Oral Buyukozturk, my thesis supervisor, and Prof. Chris Leung, my thesis advisor.

Finally, I want to dedicate this thesis to my family.

Table of Contents

List of Figures

6

List of Tables

List of Symbols

α_F	Empirical constant related to aggregate size
a	Crack length, depth of concrete compressive block
A	Paris Law constant
A_l	Area laminate
A_s	Area laminate
β_l	Concrete stress-block parameter
b	Width of beam
B	Modified Paris Law constant
c	Distance to neutral axis
δ	Displacement
d	Depth to tensile reinforcing steel
da/dN	Crack growth per cycle
δ_c	Critical displacement
d_e	Delamination location
G	Fracture energy
G_{IC}	Mode I Toughness
G_C	Toughness
G_F	Nonlinear critical fracture energy or nonlinear toughness
h	Height of film or laminate, height of beam
ΔK	Stress intensity range
ΔK_{th}	Stress intensity range threshold
ΔP	Cyclic load range
ε_l	Strain in laminate
ε_s	Strain in steel
ε_u	Ultimate strain in steel
E	Young's modulus
E_l	Young's modulus of the laminate
f'_c	Compressive strength of concrete

9

f_l	Tensile strength of laminate
f_y	Yield strength of steel
I	Moment of inertia
J_C	Nonlinear critical fracture energy or nonlinear toughness
K	Stress intensity factor
K_I	Mode I stress intensity
K_{II}	Mode II stress intensity
K_C	Fracture toughness
λ	Geometric ratio
m	Paris Law exponent
M	Moment
M_{max}	Maximum moment capacity
M_n	Ultimate moment
N	Number of cycles
P	Applied load
P_{max}	Maximum load capacity
P_f	Delamination load
Ψ	Phase angle
ρ	Steel ratio
ρ_b	Balanced steel ratio
$\rho_{blaminate}$	Balanced laminate ratio
ρ_{bsteel}	Balanced steel ratio
ρ_{steel}	Steel ratio
$\rho_{laminate}$	Balanced laminate ratio
R	Cyclic ratio
s	Spacing between shear stirrups
σ	Stress in film or laminate
σ_t	Tensile strength
Σ	Ratio of Young's modulus
V	Shear

V_c	Shear capacity provided by concrete
V_s	Shear capacity provided by steel
V_{max}	Maximum shear capacity
y	Distance to the neutral axis

INTRODUCTION

1.1 Overview

The deterioration of the nation's concrete structures creates the necessity for reliable technology for the rehabilitation of structures. The Federal Highway Administration estimates that more than 40 percent of the nation's 578,000 highway bridges are either structurally deficient or obsolete. The use of composites for the post-strengthening of concrete beams has offered an economical solution for the retrofitting and rehabilitation of damaged structures. By adhering composite laminates to the tension face of flexural concrete members, one can restore these members. This technology has already been applied effectively in Europe, South Africa, and more recently the U.S [1,2].

Although there have been many applications of strengthening with fiber reinforced plastic (FRP) laminates, many important aspects of this technology are still unfamiliar and uninvestigated. This includes distinct failure mechanisms, long-term behavior, and resistance to cyclic loading. Of these distinct failure mechanisms, brittle peel-off of the laminate from the concrete appears to be a common failure mode and an important consideration in post-reinforcement design. In fact, peel-off failure often proves to be a controlling factor in design [3]. The interfacial fracture mechanisms that govern peel-off failure require further examination.

In addition, there is still much to be studied regarding the fatigue resistance of concrete retrofitted with these laminates. There has been extensive research examining

the fatigue behavior of these post-reinforced beams under environmental cyclic loading (Chajes et al. 1994 [4]) and the fatigue strength of these beams under cyclic loading (Inoue et al. 1996 [5]). However, most research focuses on the decreasing beam stiffness and the overall deterioration of the interfacial bond between the laminate and concrete. Experience shows that shear and flexural cracks can cause peel-off of the laminate which can lead to brittle failure. Thus, there is a critical need for research into peel-off failure mechanisms under fatigue conditions. Using a fracture mechanics approach, one can study the characteristics of interfacial failure. This research will provide some insight into peel-off failure mechanisms under high-intensity cyclic loading.

This research attempts to develop a deeper understanding of the fatigue properties of the interfacial bond. Additionally, this study will include material properties related to the cyclic resistance of the FRP laminate-concrete interfaces as dictated by the Paris Power Law. This will be achieved through a series of high-intensity/low-frequency cyclic loadings on open sandwich beams. Variations in laminate materials and construction techniques will be examined. Using this data, one can characterize the behavior of the bond under high-intensity/low-cycle loading, as under earthquake loading. These results will assist in the development of service life predictions, improvements in construction techniques, and further suggestions for research.

1.2 The Use of FRP to Retrofit

Since 1967, it has been possible to post-strengthen reinforced concrete (RC) through the adhesion of steel plates. Often, RC members, cracking in tension, have exposed and corroded steel reinforcement. A beam with damaged elements cannot perform in a safe or stable manner. However, by post-strengthening these tension zones with steel plates, the member can regain its original structural integrity.

In 1970, research began at EMPA (Swiss Federal Laboratories for Materials Testing and Research) to study the use of these steel plates on concrete beams. After some time, the steel plates were corroding, effectively rendering the technology unreliable and uneconomical for application. In 1982, Urs Meier began research on the

13

use of fiber reinforced composites instead of steel plates for post-strengthening of RC [6]. In the ensuing period, comprehensive research has demonstrated FRP retrofitting to be a viable method for structural rehabilitation and improvement.

1.3 Characteristics of Fiber Reinforced Plastics

FRPs, originally developed for the aerospace industry, are composite materials, offering a combination of qualities that cannot be attained by conventional building materials such as woods, metals, or ceramics. FRPs are composed of thin fibers, usually carbon, glass, aramid, or boron, held in place within an epoxy resin matrix. The fibers are high strength, low weight, and corrosion resistant. The epoxy resin matrix preserves the fibers in their proper alignment while protecting the fibers from damage. By integrating the properties of more than one material successfully, FRPs provide various characteristics such as higher strength, superior toughness, excellent strength-to-weight ratio, corrosion resistance, effective fatigue resistance, and other features advantageous for construction purposes.

The high cost of FRPs often seems to be a major disadvantage of FRP use. Compared to steel plates, the price differential per unit weight can be substantial. However, when the superior tensile performance, ease of application, and speed of application is taken into account, the use of FRPs may actually be more economical. Because of the high strength of these materials, relatively modest amounts of laminates are required, and are easily installed with fewer workers. Additionally, post-reinforcement with FRPs causes less disturbance to the environment (and traffic) than other repair methods.

1.4 Failure Modes of RC Beams Post-Strengthened with FRP

Classical failure modes of beams are accounted for in current beam design. The most common of these failure modes are yielding of the longitudinal steel in tension, crushing of the concrete in compression, and shearing of the concrete. However, RC

14

beams retrofitted with FRP require new design criteria which recognize the specific failure modes of these altered beams.

Studies by Meier [2] have illustrated the six unique failure modes observed in RC beams post-strengthened with FRP:

a) Rupture of the FRP laminate

b) Classical concrete failure in the compressive zone of the beam

c) Peeling-off of the FRP laminates due to an uneven concrete surface

d) Shearing of the concrete in the tensile zone

e) Interlaminar shear within the FRP laminate

f) Failure of the reinforcing steel in the tensile zone (only observed during fatigue tests)

Tests performed for this research program reveal that the failure modes shown in Figure 1.1 are most commonly observed: FRP rupture, concrete compression failure, delamination of FRP, and shear failure.

a) FRP rupture   b) Concrete compression failure

c) Delamination of FRP   d) Shear failure
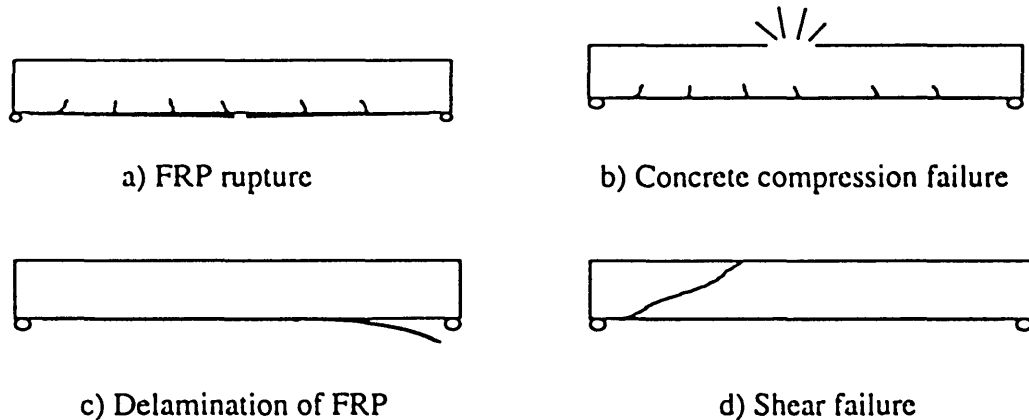
Figure 1.1: Failure Modes of RC Beams Retrofitted with Laminates

FRP rupture, which in turn causes yielding of the tensile steel, is the preferred mode of failure since this is ultimately a ductile failure. This type of failure can be planned through proper design and calculation of reinforcement ratio, thus preventing the

possibility of concrete compression failure. Shear failure can also be avoided by limiting the load level on existing shear reinforcement or even retrofitted shear reinforcement. However, delamination failure can be difficult to anticipate and prevent with current design knowledge. While a delamination failure will most likely induce ductile failure through yielding of the tensile steel, delamination will prevent the retrofitted beam from attaining its designated potential. Additionally, delamination may cause unforeseen damage which can ultimately provoke brittle failure.
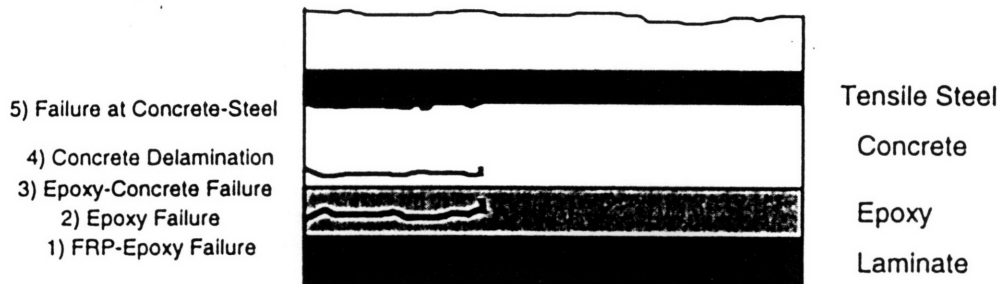
Figure 1.2: Location of Failure of the Concrete-Laminate Interface

1.4.1 Concrete-Laminate Bond Failure

Used in the context of this research program, the failure of the concrete-laminate bond implies the weakening of the concrete-laminate region to the point where the laminate can no longer transfer stress to the beam to aid in the flexural reinforcement of the retrofitted system. That is, any damage that the beam endures that renders the FRP laminate obsolete can be defined as a failure of the concrete-laminate bond. This failure often manifests itself in the region of the bond as one of several types of cracking or separation patterns:

1) Failure of the adhesion between the FRP and the epoxy
2) Cohesive failure of the epoxy
3) Failure of the adhesion between to the epoxy and the concrete

4) Delamination of the CFRP through a thin layer of concrete directly above the epoxy

5) Other failures of the concrete which weaken the concrete-laminate bond; this can include shearing of the concrete or debonding between the concrete-tensile steel layer.

The locations of these various interface failure locations are shown in Figure 1.2. Generally, this failure occurs through the concrete in one form or another, initiating as a delamination though a thin layer of concrete above the laminate. Accordingly, all of these failures will be referred to as peel-off failure, cracking, delamination or failure of the concrete-laminate bond.

1.4.2 Factors that Initiate Delaminations

Often, delamination propagation or unstable peel-off failure is promoted by the existence of initial delaminations. Initial delaminations can occur at the concrete-laminate interface for a variety of reasons. It is suggested that severe shear cracks can initiate these initial delaminations [2]. The vertical displacements caused by the shearing action can initiate laminate peel-off. This type of behavior is exhibited in Figure 1.3.

Figure 1.3: Peeling of the Laminate Due to Shear Cracking

These initial delaminations may also be caused by concrete spalling. As structural integrity of the concrete on the tension face of the beam is compromised by spalling, the bond strength is altered accordingly. Poor application of the laminate, such as improper concrete surface preparation, can also initiate delaminations. Vandalism can even be a

cause of delaminations. This laminate-concrete bond can easily be destroyed by even relatively small pulling forces applied to the laminate.

Initial delaminations can also occur on a microscopic level in the concrete. Crack nucleation, the initiation of cracks from cyclic loading, may cause initial delaminations. Furthermore, residual stresses caused by temperature gradients during cooling will initiate microcracks. Both crack nucleation and microcracking will occur at grain boundary facets, the weakest region of the molecular structure.

Initial delaminations at the concrete-laminate interface are extremely important considerations for the design of retrofitted RC beams. Initial delaminations can also instigate delamination failure for a number of reasons. First, the delamination reduces the bond area between the laminate and the concrete, in turn decreasing bond integrity. Second, the delamination usually propagates into a higher moment/shear region. This higher moment/shear will create higher stresses in the laminate, increasing the propensity to delaminate.

1.5 Objectives

The objective of this work is to develop an understanding of the fatigue behavior of the concrete-laminate interface. This research will use a fracture mechanics based approach to develop criteria controlling the failure of this concrete-laminate bond. Alternatively stated, using a fracture mechanics approach, the delamination at the concrete-laminate interface will be considered and modeled as a crack.

Pre-delaminated specimens will be loaded under static and cyclic loading to study the propagation behavior of initial delaminations in this post-reinforced beam system. Specifically, three aspects of the fracture behavior of the concrete-laminate interface will be investigated:

1. A comparative study of how laminate types and surface preparation affect peel-off failure under static and cyclic loading.

2. Static load testing to investigate peel-off failure modes and to develop a criteria for cyclic load testing.

3. Cyclic load testing to create a broader understanding of behavior under high-intensity cyclic loading and to yield Paris Power Law constants.

1.6 Outline of Thesis

This work is divided into six chapters with emphasis placed on chapters 2, 4, and 5. Chapter 2 discusses the technical background associated with this research. This section also incorporates a literature survey, mostly involving topics related to the analytical aspects of this research program. This section begins with a discussion of concepts in fracture mechanics and fatigue crack propagation. Next, assumptions related to the fracture and fatigue behavior of concrete are presented. Given the proposed assumptions, a modified Paris Power Law to describe crack propagation is established. Having introduced the significant technical information, the specific objectives of the thesis are discussed.

Chapter 3 discusses the developments in FRP post-reinforcement that apply to this research program. Antecedent research is reviewed, focusing on significant findings and implications for further research. The static and cyclic loading of post-reinforced beams is examined. Next, the fatigue behavior of FRPs is examined. Finally, this section discusses fracture mechanics research that applies to the peel-off behavior of this RC system.

Chapter 4 presents the experimental program. Topics include specimen design, material properties, and test set-up for the static and cyclic tests. Specimen design calculations are shown, analyzing load capacity for different failure modes. The technique for lamination is also discussed.

Chapter 5 reviews the results of the experimental program. The comparative study of the test variations, the development of static load test results, and the cyclic load test outcomes are among the subjects included.

Finally, Chapter 6 reviews the test results and analysis. Conclusions are drawn, especially to develop suggestions for improvements in post-reinforcement application. Additionally, recommendations are made for further research.

MECHANICS OF FRACTURE AND FATIGUE

2.1 Overview

The design of structures, such as beams or bridges, attempts to fulfill three different criteria: strength, rigidity, and longevity. The strength of a structure should be capable of supporting service load levels and should not fail under ultimate load levels. The stiffness limits deflections to ensure serviceability and curb damage. Additionally, the structure should endure for a specified time period, resisting the effects of cyclic loading, creep, and environmental damage. Traditional methods of structural design use the yield or tensile strength of materials to determine their design capacity. For example, a material is mistakenly assumed to be satisfactory if its strength is greater than the applied stress. This approach neglects the possibility of catastrophic failure by fracture.

2.2 Linear Elastic Fracture Mechanics

Fracture mechanics, originated in 1920 by Griffith, is the study of the conditions surrounding a crack tip. (In regards to this research program, the delamination will be considered and modeled as a crack.) Cracks can originate in a structure for a variety of reasons including pre-existing internal flaws, crack nucleation under cyclic loading, or surface damage during handling or construction. These cracks can then grow in an unstable manner, called fast fracture, causing catastrophic failure of the structure. The

Griffith crack theory presented in 1920 suggests that cracks in materials will propagate if the energy released by crack growth is greater than the energy required to create new crack surfaces.

The criteria governing the stability of the crack can be described by a stress intensity factor, K. K, measured in units of stress·$\sqrt{\text{length}}$ (e.g. ksi·$\sqrt{\text{in}}$), is a function of the load applied, the specimen dimensions, and the size and orientation of the crack. K is directly proportional to the stress at the crack tip. The quantitative effect of the geometry of the specimen and the crack can be quite difficult to evaluate for more complicated specimen configurations and crack orientations. Similarly, crack stability can be described in terms of fracture energy, G. G, measured in units of work/area (e.g. kips·in/in^2), is related to K as follows:

$$G = \frac{K^2}{E}$$ 　　where E is the Young's modulus of the material　　(2.1)

K_C, the fracture toughness of the material, is a material constant describing the resistance of the material to crack propagation. Lower K_C values mean that the material is brittle, while higher values of K_C imply ductility. K_C depends on the temperature at the crack tip, geometry of the section, and rate of loading. If the stress intensity at the crack tip is greater than or equal to the fracture toughness, the crack will propagate in an unstable manner:

$$K = K_C$$ 　　will initiate fast fracture　　(2.2)

Similarly, G_C is the toughness of the material. If the fracture energy applied to a specimen is equal to the toughness, the crack will propagate unstably. In this way, fast fracture can be predicted for certain material and specimen configurations. By ascertaining the fracture toughness of a material, one can prevent the fast fracture of this material through proper planning and design.

Material behavior with respect to crack propagation can be characterized as ductile, for materials such as metals, or brittle, for ceramics or glass. When a crack is

22

present in a loaded material, the crack causes a stress concentration at the crack tip. As this stress concentration reaches the yield stress of the material, the material flows plastically at the crack tip. As the material flows around tiny inclusions, impurities contained in most metals, cavities are formed near the crack tip. As plastic flow continues, the crack tip extends through these cavities. The linking of cavities is called ductile tearing. Because of this plastic zone, an initially sharp crack is blunted, consuming a lot of energy in the process. Thus, ductile materials are much tougher than brittle materials.

Fracture in brittle materials is called cleavage. Cleavage involves little or no plastic deformation at the crack tip, and therefore no crack tip blunting. Crack propagation occurs at an atomic level, as interatomic bonds are broken. The energy required to cause cleavage is little more than the energy needed to break the interatomic bonds, since little plastic deformation occurs.

MODE I:
Tensile Opening

MODE II:
In-plane Shearing

MODE III:
Anti-plane Shearing
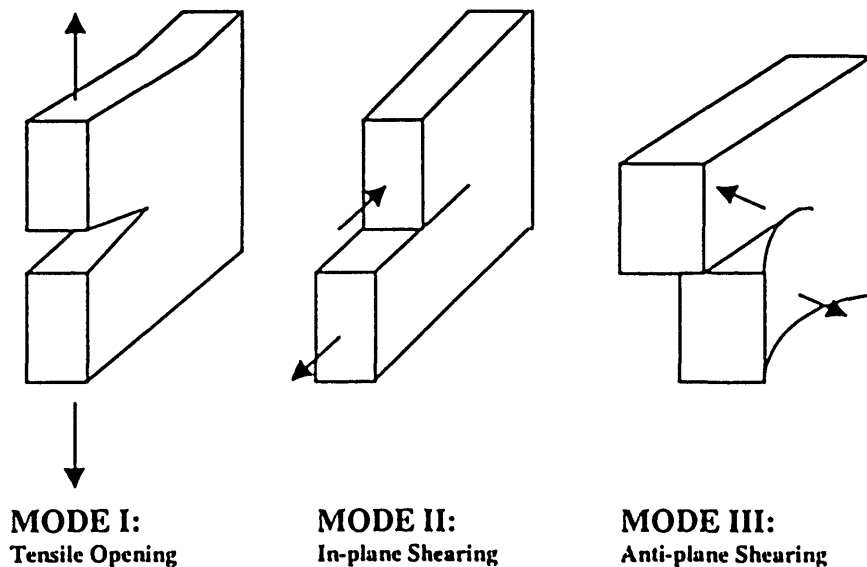
Figure 2.1: Modes of Fracture

An important aspect of the stress intensity factor is mode of fracture. The three modes of fracture are shown in Figure 2.1. Normal stresses bring about an opening mode, or mode I loading. Mode II, also called the sliding mode, is caused by in-plane shearing

with the displacement of the crack surfaces in the plane of the crack. The tearing mode, also called mode III, is caused by anti-plane shearing.

The fatigue crack resistance properties of a given material may differ under different modes of fracture:

$$K_{IC} \neq K_{IIC} \qquad (2.3)$$

where K_{IC} and K_{IIC} are the fracture toughnesses under mode I and mode II conditions respectively. Mode I is considered the most important mode for engineering applications. Generally, a crack under mixed-mode loading will reorient itself to mode I propagation.

2.3 Fatigue Crack Propagation

As discussed, if the stress intensity factor at a crack tip is greater than or equal to the fracture toughness in the material, the crack will propagate in an unstable manner. However, this crack can still propagate in a stable manner at stress intensity levels less than the fracture toughness of the structural material, $K < K_C$. If a structure is subjected to cyclic loads or destructive environments, cracks may grow even at values of K well below K_C. Fatigue is the formation and stable propagation of cracks under fluctuating stresses. Although environmental factors that lead to crack propagation are excluded from this discussion, they are important considerations in design.

There are many types of fatigue behavior. Fatigued structures can be grouped into cracked or uncracked components. Fatigue of material components can be characterized as high cycle fatigue or low cycle fatigue. These fatigue categories, as described by Ashby and Jones, are summarized in Table 2.1 [7]. This research project focuses on the fatigue of pre-cracked structures. These pre-cracked structures will be subjected to low-cycle/high-intensity fatigue.

```
                    ┌─────────────────┐
                    │     FATIGUE     │
                    └─────────────────┘
```

Fatigue of uncracked components	Fatigue of cracked structures
No cracks pre-exist; initiation-controlled fracture. Examples: almost any small components like gudgeon pins, ball races, gear teeth, axles, crank shafts, drive shafts	Cracks pre-exist; propagation controlled fracture. Examples: almost any large structure, particularly those containing welds: bridges, ships, pressure vessels.

High cycle fatigue	Low cycle fatigue
Fatigues at stresses below general yield; > 10^4 cycles to fracture. Examples: all rotating or vibrating systems like wheels, axles, engine components	Fatigues at stresses above general yield; < 10^4 cycles to fracture. Examples: core components of nuclear reactors, air - frames, turbine components, any component subject to occasional overloads

Table 2.1 Categories of Fatigue

Once initiated, cracks in ductile materials can propagate stably under cyclic loading by a mechanism of reversed cyclic slip in the plastic zone at the crack tip [8]. During the tensile cycle, a large stress concentration at the crack tip causes slip along favorably oriented slip planes. The crack tip opening displacement (CTOD) increases to an amount, δ. A new crack surface is created as the CTOD increases. The compressive cycle contracts the CTOD, folding the crack surface and extending the crack by an amount roughly equivalent to δ. When a cyclically loaded material contains inclusions, voids are created by these impurities, inducing faster crack growth. Concrete is a quasi-brittle material, meaning its fracture and fatigue crack propagation is dictated by a process zone, analogous to the plastic zone in metals. The process zone in concrete is discussed in subsequent sections.

2.3.1 Paris Power Law

Cracking always occurs in large structures, such as bridges or beams. While the location and number of these cracks are difficult to evaluate precisely, the length of these cracks will be less than the length that can be reasonably detected. Given this

conservative initial estimate of crack length, one can estimate how long the structure will be functional before the crack grows to an unsafe length.

After an initial crack is induced, this crack will grow in fatigue under cyclic loading. The rate at which this delamination (or crack) grows is determined by the stress intensity factor. The rate of growth of a crack subjected to constant amplitude stress cycles is expressed in terms of crack length increment per cycle, da/dN. Figure 2.2 shows typical behavior of crack propagation as a function of ΔK, the difference in maximum and minimum stress intensities applied in cyclic loading.
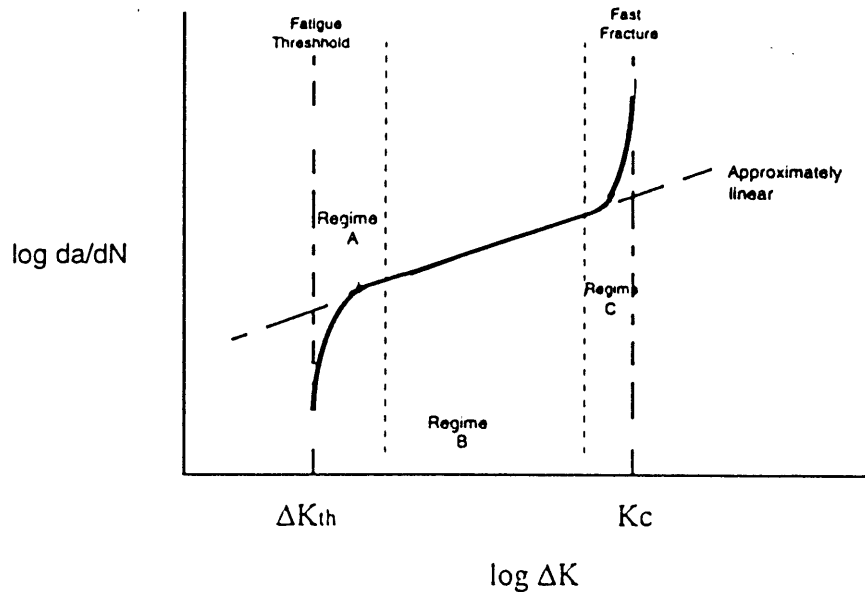
Figure 2.2: Fatigue Curve [7]

This curve can be separated into three regions. Regime A describes fatigue cracking in the low stress intensity region. Below a threshold value, ΔK_{th}, no crack growth is induced. Regime B is the intermediate stress intensity region. The curve appears approximately linear on the log-log fatigue curve. Regime C is the high stress intensity region, characterized by a change in slope. The crack growth rate increases rapidly as the stress intensity cycle approaches the fracture toughness of the material. At stress intensity ranges above the fracture toughness, the material will fracture.

The Paris Power Law, an empirical equation, is used for the analysis of cyclic crack growth for Regime B. The Paris Power Law is given by:

$$da/dN = A(\Delta K)^m \tag{2.4}$$

where $\Delta K = K_{max} - K_{min}$, da/dN is the crack growth per cycle, and A and m are empirical constants. The Power Law constants A and m are material properties that can be used to estimate the cyclic life of the tested material, or the concrete-laminate interface in this research program. These parameters, once assessed, will allow a more complete characterization of fracture criteria in the interface and a computation of the cyclic stresses that can be applied to the interface.

Table of Paris Exponents		
Material	**Paris Exponent (m)**	**Constant (A)**
Average Steel	3	1E-11
Structural Steel	3	4E-11
Forging Steel	2-3	1E-11
Ti alloy (IMI 834)	5	1E-11
Concrete	10.6	1E-18 to 1E-16

Table 2.2: Table of Paris Exponents

Of the two constants, the Paris exponent, m offers more insight into material behavior. The Paris exponent describes how crack growth is affected by changes in stress intensity range. A lower value of m implies that the material is relatively unaffected by changes in the stress intensity range. A, the Paris constant, suggests the scope of the crack growth. This constant, however, is highly susceptible to variability due to a number of parametric changes in the specimen, environment, or loading history. The Paris exponent is relatively more stable. Accepted values of Paris constants, related to units of MPa and meters, are shown in Table 2.2 [9,10].

As evident from Table 2.2, fatigue crack growth in steel is much less sensitive to changes in stress intensity range. A low Paris exponent implies good resistance to fatigue crack propagation. Additionally, it is shown that the Paris constant is not consistent in concrete. Bazant and Xu argue that the Paris constant for concrete is highly dependent on specimen geometry [10]. Their tests suggest Paris constants in the range of $10^{-18}-10^{-16}$

for concrete. However, the Paris exponent remains consistent in the 9-11 range.

Although the Paris Law offers a way to fit fatigue crack propagation data, there is still some interpretation required. The Paris Power Law is an empirical equation, having no physical basis. Thus, the Paris Law should not be accepted unquestioningly. The curve fit of fatigue data by the Paris Law using a least squares regression may not offer the most appropriate curve fit. In fact, Broek suggests that one should draw a curve fit through fatigue data by hand [11]. Regression fits weight each data point equally. However, Broek argues, some data points are more significant. The problem with a hand-drawn curve, is that there is too much subjectivity. Thus, this research program will use a regression to objectively analyze fatigue data, despite its shortcomings.

Another concern in curve fitting fatigue crack propagation data is the high degree of scatter [12]. Fatigue tests exhibit significantly more scatter than static tests [13]. First, many different parameters, such as environmental conditions, can affect or skew the consistency of fatigue data. Seemingly minor inaccuracies in crack length measurements can also cause significant scatter. Also, fracture mechanics focuses on local failure. Inconsistencies inherent in all materials, such as flaws or inclusions, can influence fatigue data. This type of inconsistency is even more pronounced in concrete, which is an inhomogeneous material.

2.3.2 Factors Affecting Crack Propagation

A countless number of factors can influence crack propagation testing. Unfortunately, test conditions often differ significantly from service conditions. These various parameters can have a significant influence on crack propagation affecting the consistency of crack propagation data.

There are many factors which can affect crack propagation, some more easily accounted for than others. The following list considers some of the factors which can affect crack propagation:

    1) Specimen variations

28

a) Geometry

b) Materials

c) Manufacturing techniques

2) Environmental variations

a) Temperature

b) Other ambient conditions

3) Loading variations

a) Frequency

b) Load history

c) Variable amplitude loading

Since the effect of some of these factors on the cracking behavior of concrete is sometimes unfamiliar, these factors are discussed in the context of established knowledge of crack propagation in metals. A subsequent section in this report will review information concerning factors that affect fatigue strength of concrete.

When testing crack propagation in metals, thickness is an important consideration since it can affect the mode of propagation. Research has shown that fatigue cracking can occur at higher rates in thicker specimens [14]. This is due to the influence of the size of the plastic zone, the plastically deformed region at the crack tip. The fatigue tests for this research program, however, are performed on FRP retrofitted RC beams, not steel samples. Thus, the plastic zone size effect would not be applicable. However, the geometry and size of the beams may affect the fatigue resistance of the concrete-laminate bond, especially when considering the concrete's process zone, the subcritical cracking region that precedes macrocracks. It has been shown that the process zone can affect the fracture toughness for different concrete beam sizes [15]. Bazant and Xu also reveal how stress intensity factors for concrete cracks may only be applicable to one specimen size or asymptotically for very large specimen sizes due to the process zone effect [10]. It is not known how geometry and the process zone affect the fatigue resistance of the concrete-laminate bond in this research program's specimen configuration. However, it is hypothesized that thickness and the concrete process zone do not have a significant effect on test results since lamination length remains notably larger than aggregate size

throughout the testing process, effectively creating a large specimen for continued crack propagation. Size effect is a parameter that should not be discounted, nonetheless.

Many other variations in specimen construction, such as construction materials or construction methods, can scatter results. In the context of metals testing, these variations include differences in heat treatment, quenching, aging, etc. In the context of laminate-concrete bond testing, many specimen variations can affect crack propagation. This includes concrete mix ratios, steel reinforcement, laminate type, lamination surface preparation, epoxy type, concrete curing duration, etc. This research program investigates the effect of two of these factors, lamination surface preparation and laminate type. It is suggested that other construction parameters be investigated in order to develop possibilities for improvements in retrofitting techniques.

Temperature is a very important factor for crack propagation in metals. It has been shown that elevated temperatures promote crack propagation [16]. Broek suggests that the faster reaction kinetics at higher temperatures prompt crack propagation [12]. Although concrete is a quasi-brittle material, not a ductile material like steel, higher temperatures and faster reaction kinetics should promote crack propagation in concrete. Other ambient conditions, such as moisture, temperature cycles, or the presence of certain chemicals, can also affect crack propagation in concrete.

Loading variations, such as frequency variations or differences in load history, are another important parameter for crack propagation. Nibkin and Webster demonstrate how frequency can affect crack propagation in metals [17]. As frequencies increased, cracks propagated at slower rates. At higher frequencies, crack propagation rate was relatively insensitive to changes in loading frequency. This type of behavior is displayed in Figure 2.3.
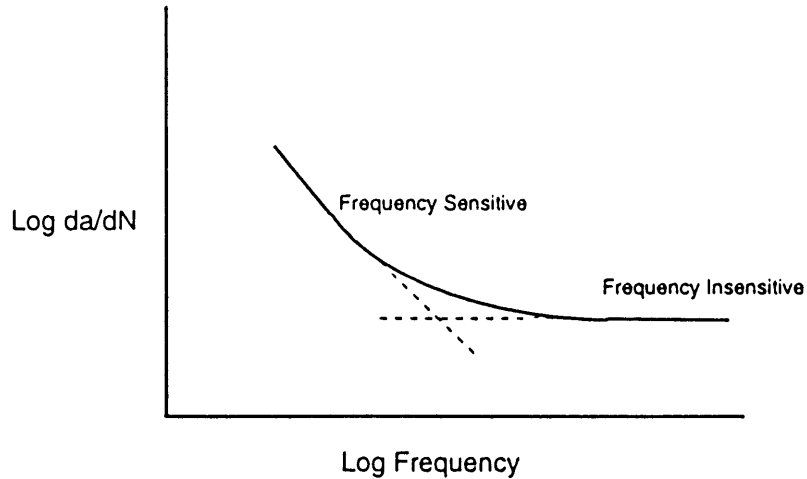
Figure 2.3: Frequency Dependence of Crack Growth per Cycle

Variable amplitude loading can also influence crack propagation. Applied overloading in constant amplitude testing has been shown to retard crack propagation in steel [18]. Overloading induces residual compressive stresses at the crack tip, which resist crack tip opening. A similar mechanism may occur in concrete crack propagation testing. Overloading in concrete will augment the process zone, toughening the concrete in the crack tip region. Thus, any prior overloading in retrofitted RC beam testing may alter crack propagation results.

The parametric possibilities involved in the specimen, environmental conditions, and load histories for a research project such as this are endless. While most parameters were accounted for, it is difficult to assess the applicability of the results of this program to other retrofitted structures. However, it is more important to gain insight into general peel-off mechanisms and concepts than to develop statistics.

2.4 Fracture Mechanics of Concrete

The fracture of concrete differs significantly from that of metals and glass, which are ductile and brittle materials, respectively. Concrete is a quasi-brittle material, tougher than most ceramics, which are considered brittle materials. While concrete cracks in a

brittle fashion, it gains toughness from its process zone, the subcritical cracking region that precedes macrocracks. The following section discusses this process zone.

Due to this process zone, the use of linear elastic fracture mechanics is inappropriate for the analysis of concrete behavior. Instead, nonlinear fracture methods, or elastic-plastic fracture mechanics, should be utilized in order to account for the non-linear behavior of the process zone. The nonlinear behavior of concrete is discussed further in Section 2.6.
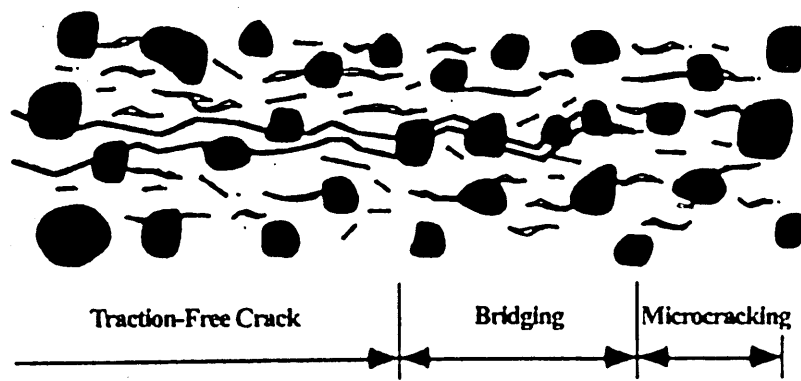
a) Crack Growth in Concrete
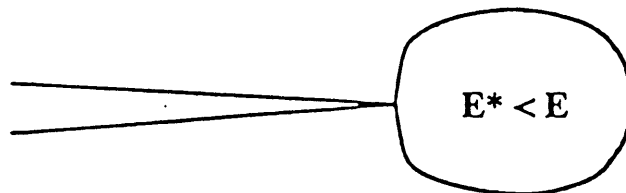
b) Process Zone Idealized as a Strain Softened Zone
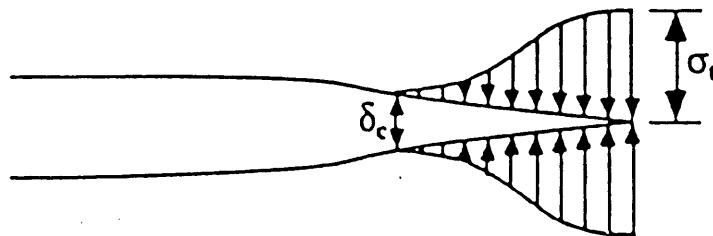
c) Process Zone Idealized by Closure Tractions

Figure 2.4: Process Zone in Concrete with Two Simplified Models [15]

2.4.1 Process Zone in Concrete

The concrete fracture process zone, shown in Figure 2.4, consists of two parts: microcrack formation ahead of a macrocrack and an aggregate bridged region behind the macrocrack tip. The bridging occurs as the weak interface between the matrix and the aggregate begins to deteriorate. While the crack tip may appear to discontinue with the traction-free zone, the process zone influences the fracture behavior. Conventional linear elastic fracture mechanics unsuccessfully models concrete cracking because of this process zone.

There are two approaches to modeling concrete cracking behavior. Figure 2.4 displays two idealizations of the process zone. The process zone can be represented as a lower modulus region (Fig. 2.4(b)). Alternatively, the process zone can be modeled as a longer crack with closure tractions represented as crack closing stresses, as shown in Figure 2.4(c). Both these models, however, require knowledge about the size of the process zone. This can be achieved through crack mouth opening displacement measurements. This type of measurement would be difficult to perform on the specimens of this research program.

This process zone makes the determination of the stress intensity at the crack tip and the location of the true crack tip extremely difficult. However, this research program circumvents the necessity for this information. As discussed in a subsequent section, a stress intensity value is not used. Instead, a method of estimating relative stress intensity is employed. Additionally, the estimation of the crack tip location uses the location of the macrocrack tip. Thus, while there may be an error in the determination of the crack tip location, this error is constant and cancelled out when crack growth is estimated. As long as the error is consistent to one side, it would result in a shift of the crack locations, but not the crack growth rates [11]:

$$\frac{a_2 + \delta - (a_1 + \delta)}{\Delta N} = \frac{a_2 - a_1}{\Delta N} = \frac{\Delta a}{\Delta N} \tag{2.5}$$

where ΔN is the number of load cycles, δ is the measurement error caused by the process zone, and a_1 and a_2 are beginning and end crack lengths, respectively. As shown in equation 2.3, the error in crack length measurement caused by the process zone cancels out, as long as the error is consistent to one side. The crack propagation rate measurement remains relatively accurate. Thus, it is proposed that the process zone effect should not have a major influence on this research program's results. However, as suggested, size effect issues should still be investigated.

This process zone effect also creates a discrepancy in concrete fracture toughness under static and cyclic loads. Research has shown that the fracture toughness of concrete obtained from specimens loaded in fatigue differs from that of concrete tested statically [19, 20]. Swartz et al. show how concrete loaded in fatigue has a lower fracture toughness than statically loaded concrete [20]. However, Swartz's research also exhibits how this discrepancy in fracture toughness is insignificant. Therefore the static fracture toughness of concrete will be used to estimate the fracture toughness of fatigue concrete. Nonetheless, this difference in fracture toughness under fatigue and static loading does merit further investigation.

2.4.2 Factors Affecting Concrete Fatigue Strength

While there is often little conclusive data on how different parameters affect crack propagation in concrete, there has been extensive research on the effect of various parameters on concrete fatigue strength. Fatigue strength determines how the strength of an uncracked concrete structure is affected by cyclic loading. While fatigue strength and fatigue crack propagation are not equivalent concepts, fatigue strength is related to how the cohesive bonds between concrete's numerous elements, such as aggregate or mortar, deteriorate under loading. Thus, one may infer that if a parameter affects concrete fatigue strength, this same parameter may affect crack propagation in a similar way. For this reason, this section discusses some important variables that will affect concrete fatigue strength.

Fatigue tests on concrete have included variations in loading history, specimen preparation, and environment [13,21-23]. Tests have shown that there are innumerable parameters that can have different effects on concrete fatigue strength. Some of the specific test variations include air entrainment, aggregate type, water:cement ratio, concrete age, moisture differentials, and detrimental chemical agents. These parameters may even interact with each other to influence concrete fatigue strength in unpredictable ways. Only the most relevant literature on concrete fatigue is reviewed in this section.

The American Concrete Institute also published findings on the effects of various parametric changes on concrete fatigue [13]. The report suggests that the range of stress will affect concrete fatigue. In this research program, it is not stress range, but stress intensity range, or cyclic range, that is the salient variable. The cyclic ratio, R, is the ratio of minimum stress intensity to maximum stress intensity:

$$R = \frac{K_{min}}{K_{max}} \tag{2.6}$$

The cyclic ratio for this research program is consistently maintained at R = 0. It is difficult to predict how results would be affected by changes in cyclic ratio.

Raithby and Galloway tested concrete beams in fatigue, varying rate of cyclic loading and length of rest periods between cyclic tests [21]. It was discovered that beams cyclically load tested up to a frequency of 20 Hz were insignificantly affected by changes in frequency. This research program cyclically loads beams at a rate of 1 Hz, well below this upper bound suggested by Raithby and Galloway. Additionally, these researchers suggest that rest periods between cyclic loadings have little effect on the fatigue strength of concrete beams. Thus, any rest periods during testing in this research program should have negligible effects on results.

2.5 Modified Paris Power Law

The stress intensity factor is difficult to determine for some structural and crack configurations. This is the case in this research program. K, the stress intensity factor which describes this loading configuration, is a function of the load (P), the location of the delamination tip (d_c), and the loading geometry. The configuration of the delamination and the beam makes ascertaining the stress intensity factor at the delamination tip very difficult for a few reasons.
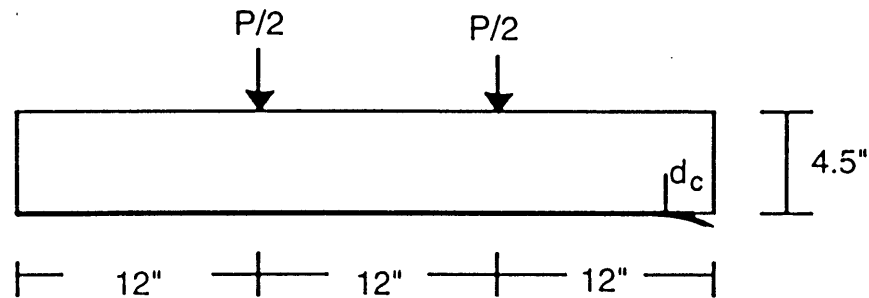
Figure 2.5: Delamination of the FRP

The general specimen configuration used for this research project is shown in Figure 2.5. The laminate peel-off is artificially induced, promoting delamination growth at the concrete-laminate interface. As the delamination propagates from the end of the beam towards the center, the shear to moment ratio changes at the delamination tip, also changing the phase angle, the ratio of mode II to mode I stress intensity factors. This will make the determination of the effective stress intensity factor at the delamination tip quite complex.

Finally, the stress at the delamination tip is required for application of general stress intensity equations. While conventional beam theory offers a general solution, the unpredictable effects of the changing moment of inertia under concrete cracking, microcracking of concrete, and beam damage under fatigue alter this solution. It is suggested that there is a transition zone at the ends of the concrete-laminate interface that

modifies the stress transfer at the interface. This hypothetical stress transition zone is depicted in Figure 2.6.
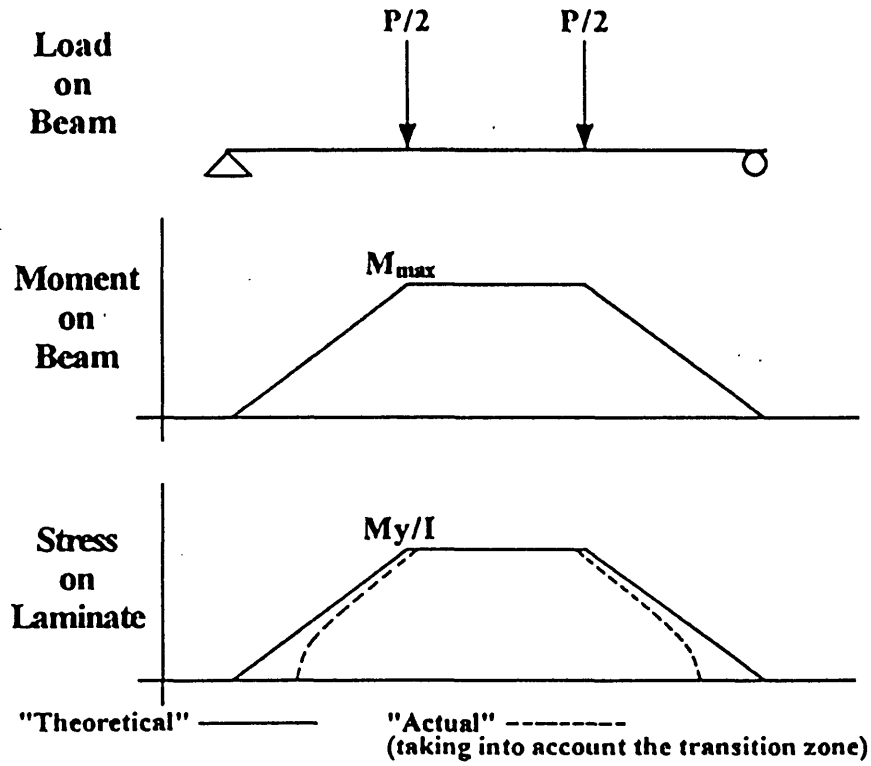
Figure 2.6: Stress Transition Zone at the Concrete-Laminate Interface

The combined effects of the numerous uncertainties in determining the stress intensity factor at the crack tip create a need for an alternative method for utilizing the Paris Power Law. (Additionally, as discussed in the next section, stress intensity factor may be an incomplete predictor of concrete crack propagation.) Thus a modified version of the stress intensity factor will be used in order to estimate the Paris Power Law constants for the interfacial region without calculation of stress intensities:

$$\frac{da}{dN} = B\left(\frac{\Delta K}{K_c}\right)^m$$

where B is a material constant   (2.7)

Since K_C, the critical stress intensity factor, is a material constant, the Paris Power Law can be rewritten in this way as suggested by Bazant and Xu [10]. This form of the Paris allows the modified Paris constants, m and B, to be independent of any possible size effects. Since all stress intensity factors are normalized by the critical stress intensity factor, K_C, this data can be applied to different sizes and different geometric configurations. However, the "regular" Power Law must be adjusted by the factor, K_C, which changes for different sizes and geometric configurations. The Power Law constant A then can be estimated:

$$A = \frac{B}{K_c^m}$$

(2.8)

As stated, K_C will be difficult to calculate accurately. However, an estimation of this stress intensity factor, or at least the magnitude of K_C, will offer an approximation of A. In order to solve $(\Delta K / K_C)$, static tests will be used to create a failure interaction curve:
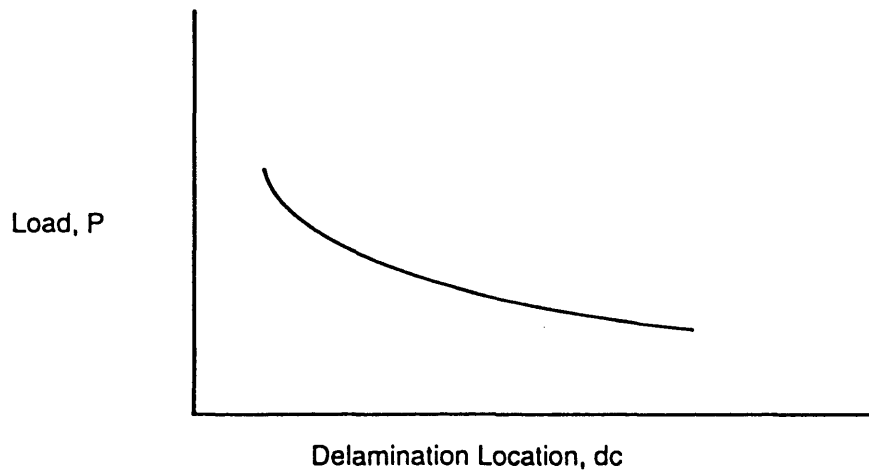
Figure 2.7: Failure Interaction Curve

For a load and delamination location combination, (P, d_c), above the interaction curve, the laminate will peel-off. It is hypothesized that each load and delamination location on the failure interaction curve represents the same stress intensity, namely K_C. Because

stress intensity is directly proportional to the load, the ratio of stress intensity range to the critical stress intensity factor can be computed in this way:

$$\left(\frac{\Delta K}{K_c}\right) = \left(\frac{\Delta P}{P_f(d_c)}\right) \qquad (2.9)$$

where ΔP is the cyclic load range, the difference between the maximum and minimum cyclic load, and $P_f(d_c)$ is the load at unstable fracture (or fast delamination) for a given delamination location, d_c. P_f is also called the delamination load, the load required to initiate delamination of the FRP laminate. Equation 2.9 does not take into account the nonlinear behavior of concrete (i.e. process zone effects). However, using this estimation will allow a rough calculation of the Paris Power Law constants. The Paris Power Law can then be rewritten:

$$\frac{da}{dN} = B\left(\frac{\Delta P}{P_f(d_c)}\right)^m \qquad (2.10)$$

which is the form of the Paris Power Law used in this research program. Therefore, instead of using stress intensity factors, which might be inaccurate or difficult to calculate, the Paris Power Law will be evaluated using delamination loads and cyclic load range. Both of these can be evaluated easily: the failure interaction curve can provide the various delamination loads, while the cyclic load range is dictated in the cyclic tests. Additionally, the multi-material (steel, concrete, epoxy, and FRP) properties of the interface can be disregarded as the modified Paris Lower Law incorporates the multi-material contributions in the delamination load. Thus, the Paris Power Law constants A and m, which describe the interfacial fatigue characteristics, can be estimated through a series of static and cyclic load tests.

2.6 Nonlinear Fracture Theories for Concrete

The bulk of this chapter has considered peel-off failure and the fracture of concrete in terms of linear elastic fracture mechanics for the sake of simplicity. This, as discussed, is incomplete due to the elastic-plastic behavior of concrete induced by the process zone. Instead, concrete fracture should be considered in terms of elastic-plastic fracture mechanics. This, however, should not affect the analysis of the modified Paris Power Law, Equation 2.10, which is applicable in the context of linear elastic fracture mechanics and nonlinear fracture methods for concrete.

Linear elastic methods discuss fracture in terms of fracture energy or stress intensity. If the fracture energy applied to a specimen reaches the toughness of the specimen (or the stress intensity reaches the fracture toughness), the specimen will fail via fast fracture. In practice, G_C does not generate the required energy to induce complete fracture. G_C does cause failure of the bond between two fracture surfaces, but does not induce complete separation. This is due to the energy dissipation in plastic deformation required by the deformation of the process zone. The total energy required for fracture, both plastic and elastic, is encompassed in the parameter, J_C (also labeled G_F), the nonlinear toughness. Theoretically, if the applied fracture energy reaches the critical nonlinear fracture energy, a specimen will fracture:

$$G_I = J_{IC} \qquad (2.11)$$

Despite standardized tests to evaluate J_C, its value is not constant, as it fluctuates for different concrete specimen sizes. Thus there is a necessity for another way to predict concrete fracture.

There are two accepted theories which predict the onset of concrete fracture: the two-parameter model proposed by Jenq and Shah [24] and the effective crack model proposed by Nallathambi and Karihaloo [25]. Both theories essentially state that the fracture of concrete will occur if the stress intensity at the crack tip is equal to the fracture toughness and if the effective crack length reaches a critical crack length:

$$K_I = K_{IC}^c, \quad a = a_c \qquad \text{will initiate concrete fracture} \qquad (2.12)$$

Alternatively stated, the theories maintain that for a given effective crack length, concrete will fail at the same critical stress intensity:

$$K_I\big|_a = K_{IC}\big|_a \qquad \text{will initiate concrete cracking} \qquad (2.13)$$

While the methods for determining the stress intensities and the effective crack length differ in each theory, the principles are similar. The stress intensities are still proportional to the applied load, while the effective crack length is a function of the applied load and the geometry. The stress intensity factors in both theories are proportional to applied load. Furthermore, the effective crack length will remain constant for a given geometry, initial crack length, and applied load. Therefore, Equation 2.13 can be rewritten:

$$P(d_c)\big|_a = P(d_c)_f\big|_a \qquad \text{will initiate concrete cracking} \qquad (2.14)$$

However, uncertainty remains in the determination of the Paris constant. The determination of the Paris constant, as given by Equation 2.8, depends on the appropriate estimation of K_C. That is, the Paris constant will change for different crack lengths, different geometries, and different failure loads, as K_C will change with these parameters. Therefore, while the Paris exponent, m, is invariant, the Paris constant, A, will vary with different specimen geometries.

In conclusion, the Paris Power law is an empirical equation. Although it is used primarily on linear elastic materials, its has been shown to model crack propagation in concrete fairly well by Bazant and Xu [9], Baluch et al. [26], and Perdikaris and Calomino [27]. Variables such as size and cyclic ratio have been shown to change the Paris constant, but not the Paris exponent [10,26]. Similarly, the modified Paris Power Law presented should offer an estimate of the Paris constants as the Paris exponent will remain immutable and the Paris constant can be calculated for different specimen configurations.

2.7 Thesis

Having reviewed the necessary technical background, the objective of this research project can be restated with respect to the framework established in this section. First, the broad objectives of the project are restated:

1. A comparative study of how laminate types and surface preparation affect peel-off failure under static and cyclic loading.

2. Static load testing to investigate peel-off failure modes and to develop a criteria for cyclic load testing.

3. Cyclic load testing to create a broader understanding of behavior under high-intensity cyclic loading and to yield Paris Power law constants.

These objectives will be achieved through a two-stage testing program. First, failure interaction curves will be formed using a series of static load tests on the pre-delaminated retrofitted beams to establish points on this interaction curve. The complete curve will then be interpolated using these experimentally ascertained points. These interaction curves will be produced for different parameter permutations, allowing parametric comparisons for statically loaded beams. Using these failure interaction curves, the Paris Power Law can be utilized in its modified form, Equation 3.8. Additionally, static load tests will yield various failure modes, possibly revealing a correlation between failure mode and specimen type.

The second stage of the project entails the cyclic load testing of pre-delaminated FRP retrofitted RC beams. Again, tests will be performed on differently prepared beams, allowing a comparison of the cyclic resistance properties of various parameters. Using cyclic test data in conjunction with static test data, Paris Power Law constants will be calculated. Again, failure modes in cyclic loading with respect to specimen type can be investigated.

Paris Power Law constants will impart information regarding the cyclic load resistance of the concrete-laminate interface: long-term cyclic load resistance, high-intensity cyclic load resistance, and service life estimations. As suggested, the Paris

constant, A, is highly unreliable since it is sensitive to the specimen geometry [10]. More importantly, however, the Paris exponent will offer insight into the interfacial fatigue behavior.

Chapter 3

LITERATURE REVIEW

3.1 Overview

There has been extensive research covering various aspects pertaining to the post-reinforcement of RC beams with FRPs or steel plates. Among the topics reviewed are the static and cyclic testing of post-reinforced systems, the fatigue behavior of FRPs, and the study of the interfacial strength of the laminate-concrete bond. These precedent research projects offer direction to this research program and will be discussed in relation to this research project. Special attention will be given to notable findings and suggestions for further research, which will frame the research objectives and experimental program.

3.2 Static Load Testing of RC Post-Strengthened with FRP

Extensive research has shown the viability of FRP post-reinforcement as a rehabilitation method. EMPA post-reinforced a 6-meter long RC T-beam with CFRP. Post-reinforced beams yielded a 32% increase in strength over unretrofitted beams [2]. Other research has revealed that glass and Kevlar based FRP laminates can increase beam strength by over 40% [28, 29]. Sierakowski et al. demonstrated that the flexural response of FRP retrofitted RC beams can be predicted through a strength of materials approach with considerable accuracy [30].

Arduini and Nanni examined how precracking altered the effectiveness of FRP post-reinforcement [3]. After preloading virgin beams to induce cracking, the researchers then fitted these RC beams with CFRP laminates. Beam size and epoxy type variations were tested. Three types of concrete surfaces were also examined: clean, sanded, and sandblasted. Despite the variation in beam preparation, peel-off failure controlled ultimate beam strength. Thus, the failure of the concrete-laminate interface must be studied in order to assure the effectiveness of FRP post-reinforcement.

3.3 Cyclic Load Testing of RC Post-Strengthened with FRP

Much research has been performed to evaluate the durability of FRP reinforced beams. Work by Chajes et al. examines the effect of environmental cycles, specifically wet/dry and freeze/thaw cycles, on FRP post-reinforced RC beams. Retrofitted beams were subjected to different environmental cycles, then tested in static loading. Laminate types included aramid, e-glass, and graphite. Results showed that concrete spalling occurred as a result of freeze/thaw cycles. Freeze/thaw damage compromised the integrity of the laminate reinforcement as evidenced by inferior deflection resistance and decreased beam capacity. In addition, aramid and graphite post-reinforced beams exhibited various degrees of peel-off failure when statically loaded after environmental cycling despite failing under different failure modes when not exposed to environmental attack. Thus, this experimental work indicates how environmental effects can promote peel-off failure.

Cyclic load testing performed by Inoue et al. studied the fatigue strength of RC beams post-reinforced with CFRP or steel plates [5]. Other beam preparation variations included anchorage of the reinforcement plates and sandblasting. Beams were cycled at 5 Hz at load ranges between 10-70% of experimental ultimate static strength. The researchers found that beams with unanchored CFRP failed by separation of CFRP from the RC beam. Beams with anchored CFRP failed by CFRP separation or fracture of the CFRP laminate. Therefore, even CFRP anchorage did not ensure CFRP adhesion. The investigation also revealed that fatigue life increases with a decrease in bond stress. This

implies that the stress in the laminate is inversely related to the number of cycles to failure of the CFRP adhesion. Equivalently, the stress intensity at the concrete laminate interface is related to peel-off rate. This work confirms the necessity of studying peel-off failure from a fracture mechanics perspective.

3.3.1 Fatigue Behavior of FRP

The fatigue behavior of the FRP is a consideration as it may control the service life of FRP retrofitted systems. However, the results presented by Inoue et. al also suggest that the fatigue strength of CFRP laminates seems to be insignificant, as the fatigue failure occurs as the CFRP peels-off from the concrete for unanchored CFRP laminates. CFRP rupture in fatigue does occur for anchored laminates [5]. However, this is induced by the local flaws at the drill holes in the laminate required for laminate anchorage. Thus, the damage created during construction prompts failure by rupture. Overall, any FRP clamping or bolting system may create large local stresses in the laminate which can promote laminate rupture. Such a system is not used for this research program.

Inoue also compares the fatigue lives of CFRP retrofitted beams to the fatigue lives of unretrofitted beams. Holding the cyclic stress range in the rebar constant, the researchers show that the fatigue lives of unretrofitted beams, CFRP retrofitted beams with anchorage, and CFRP retrofitted beams without anchorage are nearly identical. Thus the fatigue behavior of the CFRP laminate does not affect the overall fatigue life of the RC beam.

3.4 Fracture Mechanics Approach to Peel-Off Failure

While all the previous research discussed in this section offer important insight into the behavior of retrofitted RC beams, these works only allude to laminate peel-off failure from a fracture mechanics standpoint. Peel-off failure is a local failure

phenomenon, but is usually only discussed in terms of the overall fatigue strength of the post-reinforced system. Unfortunately, fatigue strength ignores the effect of existing flaws. It is essential to take into account existing flaw sizes when designing large structures; FRP post-reinforcement should not be an exception. In fact, there is little work that explores peel-off failure from a fracture mechanics approach.
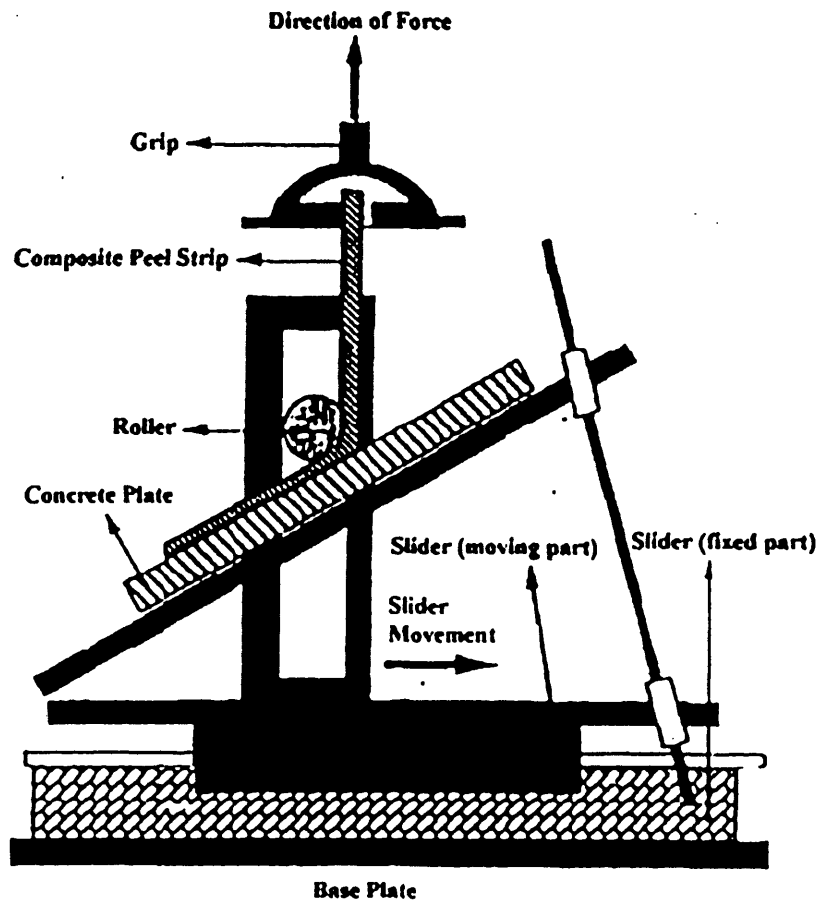
Figure 3.1: Modified Peel Test Apparatus [31]

Research by Karbhari et al. examines the interfacial fracture toughness of the concrete-laminate bond using a modified peel test [31,32]. Using a testing mechanism, shown in Figure 3.1, the researchers performed a modified peel test to examine the concrete-laminate bond. Testing small scale specimens, the experimental program varied phase angle, Ψ, which is related to the ratio of mode I stress intensity to mode II stress intensity:

$$\tan \Psi = \frac{K_{II}}{K_I} \qquad (3.1)$$

Specimens were also subjected to different environmental conditions such as immersion in fresh water, immersion in sea water, exposure to low temperatures, and exposure to freeze/thaw cycles. Test results revealed fracture energies for various phase angles and environmental conditions. It was shown that water and salt water is detrimental to bond toughness, while low temperatures and freeze/thaw cycles actually increased bond toughness. Additionally, GFRP laminate is sensitive to phase angle while CFRP laminate is not.
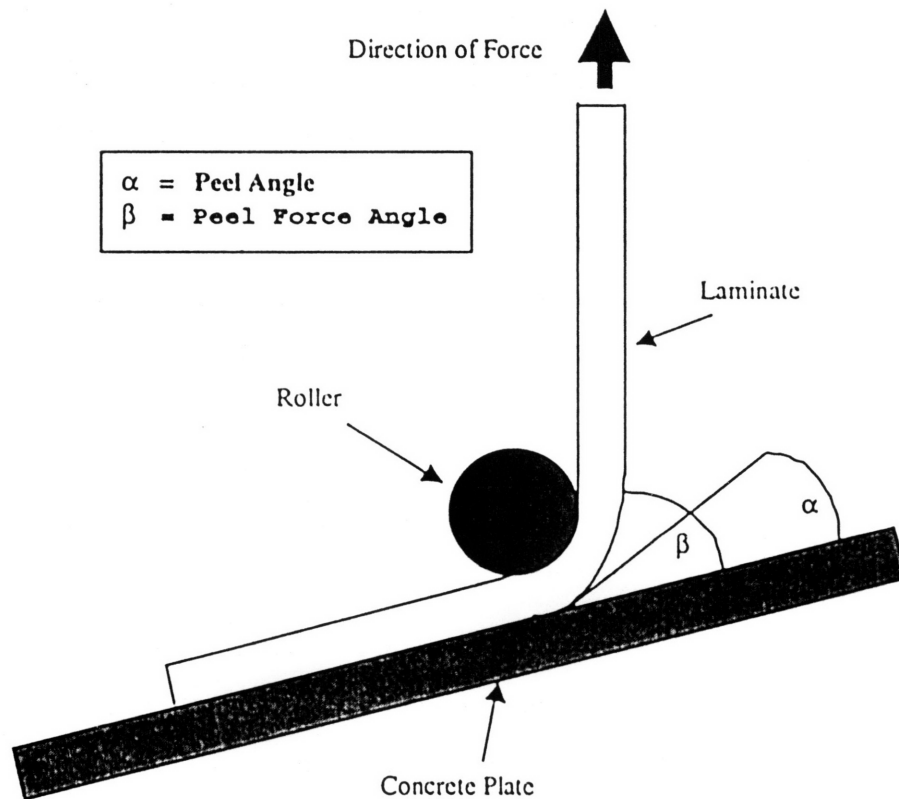
Figure 3.2: Peel Force Angle Not Necessarily Peel Angle

While the research project used an interesting approach to isolate the interface, there were still a number of ambiguities within the scope of their procedures and analyses. First, the toughness calculations yielded values higher than 400 J/m^2, even for mode I fracture. This is curious since the mode I toughness of concrete, G_{IC}, is roughly 30 J/m^2 [7]. This result implies that the concrete-laminate bond is an order of magnitude tougher than the concrete itself. In other words, the system is tougher than its individual components. Also, the bond toughness increased when exposed to low temperatures and freeze/thaw cycles, usually considered damaging environments.

Second, the measurement of the phase angle did not account for the curvature in the laminate. That is, the peel force angle did not necessarily equal the peel angle at the crack tip. This is due to the curvature of the laminate in resisting bending. This behavior is exhibited in Figure 3.2. This oversight may contribute, in part, to the peculiar toughness results as discussed previously. Hence, the application of these results to structures requires further examination. Although, the fracture energies were obtained for various phase angles, the relevant phase angle on actual structures remains to be determined, which is a difficult task.

Drory et al. suggest an equation for the fracture energy for the decohesion of residually stressed thin films from a substrate [33]. This equation estimates the fracture energy applied to the film-substrate interface:

$$G = \frac{\sigma^2 h}{E_l}\left(\frac{\Sigma}{2(\lambda + \Sigma)}\right)\left[1 + \frac{\lambda^2(\lambda + 1)^2}{4(\lambda + \Sigma)I}\right]$$
(3.2)

where G is the fracture energy at the decohesion tip, σ is the residual stress in the film, E_l is the elastic modulus of the laminate or the film, λ is the ratio of the thickness of the substrate being peeled-off to the thickness of the film, h is the thickness of the film, Σ is the ratio of the Young's modulus of the film to the Young's modulus of the substrate, and I is the moment of inertia of the peel-off strip. A depiction of the decohesion of the film from the substrate is displayed in Figure 3.3.
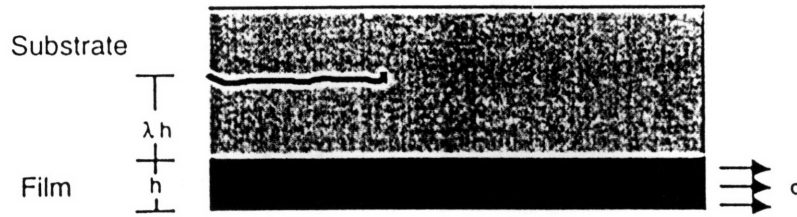
Figure 3.3: Decohesion of Film from a Brittle Substrate

Since the delamination of a thin composite laminate from the concrete is similar to the decohesion of a thin film from a substrate, the fracture energy equation can be applied to these post-reinforced beams to determine the concrete-laminate interfacial toughness. Drory's equation offers some insight into the peel-off characteristics of the concrete-laminate interface. For example, the importance of the depth of the concrete layer being stripped by the laminate peel-off, λh, is revealed. As this depth changes, the associated fracture energy changes accordingly. Unfortunately, the fracture energy equation developed by Drory et al. requires a knowledge of the stress, σ, at the delamination tip. This stress, however, is difficult to calculate using simple beam theory due to various non-linear factors, as discussed in Section 2.5. Thus, despite its potential applications to this research project, Drory's fracture energy equation is unutilized due to its limitations.

Ongoing research at MIT by Buyukozturk and Hearing investigates the fracture energy of the concrete-laminate interface using two-meter long RC beam specimens [34]. Beams are retrofitted with CFRP laminates, which are initially delaminated to various lengths along the beam. These pre-delaminated beams are then tested in monotonic loading in order to find the delamination load, the load required to induce delamination of the CFRP laminate from the concrete. Given the delamination load, one can calculate the fracture energy of the interface. The objective of their work is to develop a single parameter to predict peel-off failure. This work by Buyukozturk and Hearing serves as a basis for this research program.

3.5 Summary

The various research programs that have been reviewed have offered insight for this research program. Both static and cyclic tests have demonstrated how peel-off failure can control beam capacity. Thus, there is a necessity to study peel-off failure mechanisms. Cyclic testing has also revealed the detrimental effects of certain environments on the concrete-interfacial bond strength. CFRP fatigue properties were also demonstrated to be adequate for the retrofitting of RC beams.

Previous research, which studied peel-off failure in terms of fracture mechanics, was examined. Among the topics discussed were a modified peel-test, a fracture energy equation for decohesion, and the static testing of pre-delaminated CFRP retrofitted RC beam specimens.

EXPERIMENTAL WORK

4.1 Introduction

The previous chapters illustrated some of the shortcomings of current knowledge and understanding of the concrete-laminate interface. Thus, a new experimental program is required in order to investigate the cyclic load resistance of the concrete-laminate interface. This chapter outlines the experimental program employed in order to meet the research objectives. The experimental program is comprised of two stages: a static loading program and a cyclic loading program. The details of the various aspects of the experimental program are discussed: specimen design, material properties, specimen fabrication, and experimental set-up.

4.2 Specimen Design and Material Properties

The RC box-beam specimen used is shown in Figure 4.1. It is the model used by Buyukozturk and Hearing [34], which is a scaled down model of the one used by Deuring [6]. The beam was prepared to be monotonically and cyclically loaded in four point bending. This model was chosen because of its similarity to these previous models in order to exploit previously developed data. The unretrofitted RC specimen was designed to fail by steel yielding in tension. This specimen was projected to fail by concrete

shearing when retrofitted with CFRP and composite rupture under tension when retrofitted with GFRP. Design calculations are shown in Section 4.3.

(4) #3 Rebar

(24) .15" Stirrups

.047" thick laminate

(a) Cross Section of Proposed Box Beam Specimen

(b) FRP Post-Reinforced Beam
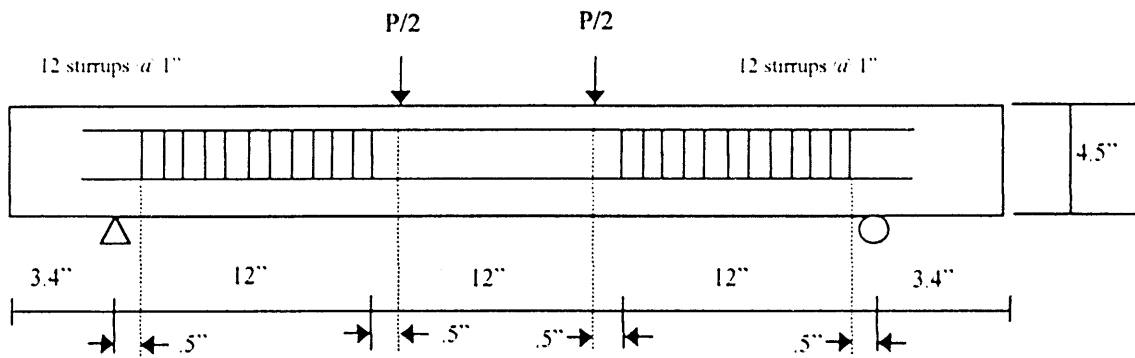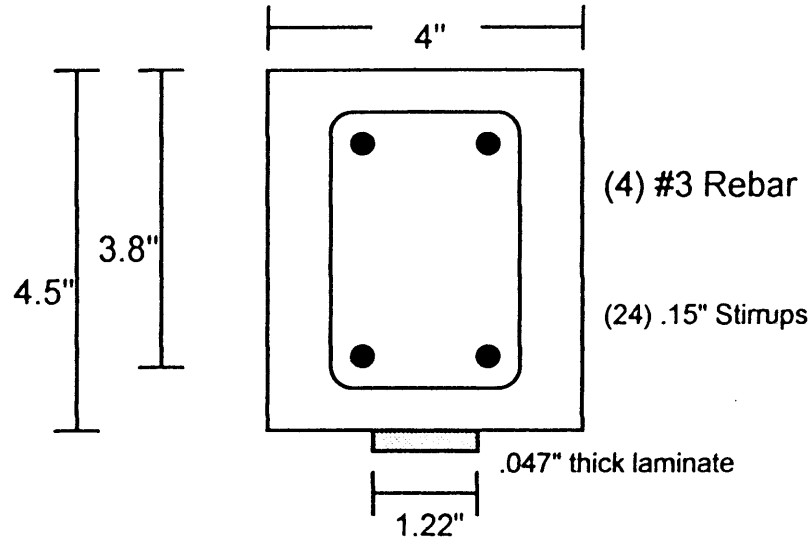
Figure 4.1: Four Point Bending on Box Beam

33 beams were constructed to be tested in static or cyclic loading. Beams were 42.8 inches in length with a 36-inch test span. Supports were placed 3.4 inches from each end of the beam. Beams were internally reinforced with 4 #3 grade 60 steel rebar. The ends of the longitudinal reinforcement were hooked 180° to ensure a proper development

length. The beam was reinforced against shear, except in the zero shear region, the middle third of the test span. The shear reinforcement consisted of 12 shear stirrups placed at each outer third of the test span. Each 36 ksi steel stirrup was .15 inches in diameter.
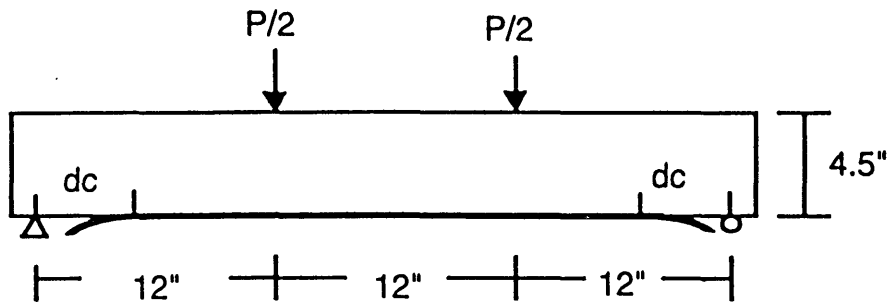
Figure 4.2: FRP Retrofitted Beam with Initial Delaminations

Except for the control beams, each specimen was post-reinforced with an FRP laminate, either CFRP or GFRP. The laminate was .047 inches thick and 1.22 inches wide. The laminate extended the length of the test span. Laminates were adhered to the concrete beam with Sika 30 epoxy. Initial delaminations at given locations, dc, were manufactured on both ends of the beams. The properties of the main material components of the specimen are listed in Table 4.1.

Material	E (Msi)	f'c (ksi)	fy (ksi)	ft (ksi)
Concrete	3.8	5.1	N/A	0.53
Steel	30	N/A	60	N/A
Adhesive (Sika 30)	0.7	8.6	N/A	3.6
CFRP (T700)	22.5	N/A	N/A	348
GFRP (G10)	4.3	N/A	N/A	50

Table 4.1: Summary of Material Properties

4.2.1 Concrete

Beams were manufactured with Type II 7-day Portland cement, mortar sand, pea gravel, and water with relative ratios of 2:4:3:1 respectively. The mix proportions used for each batch are shown in Table 4.2. Each batch yielded approximately 1500 in^3. The compressive strength of the concrete averaged 5.1 ksi. Beams were cured for one day in molds and seven days in a limewater bath. Beams were air dried for one day before FRP application and air dried for another 7 days after FRP application before being tested.

Constituent	Weight
Concrete	29.7 lbs
Sand	60.5 lbs
Aggregate	47.5 lbs
Water	14.9 lbs

Table 4.2: Concrete Mix Ratio

4.2.1.1 Fracture Properties of Concrete

Although the nonlinear toughness of concrete, J_c, has been shown to vary with specimen size, it is still a widely accepted fracture parameter for concrete [35]. The CEB-FIP Code (1993) relates the nonlinear toughness (or fracture energy) of concrete to the compressive strength:

$$J_c = \alpha_F \left(f'_c \right)^{0.7} \qquad (4.1)$$

where α_F is an empirical coefficient depending on the maximum aggregate size and f'c is measured in Mpa. Using this formula, the estimated nonlinear toughness of the concrete used in this research program was roughly 50 J/m^2 or .286 kips·in/in^2. Substituting the nonlinear toughness of concrete for G, Equation 2.1 yields a nonlinear fracture toughness of 1.04 ksi·in$^{1/2}$ (1.14 MPa·m$^{1/2}$ in metric units). This is similar to the results obtained by

Jenq and Shah [24].

It is proposed that under the given loading configuration the interface delaminates under mixed-mode conditions. (This mixed mode loading condition is considered further in Section 5.2.) Bazant and Pfeiffer estimate the mode II fracture energy of concrete to be 25 times larger than mode I fracture energy [36]. This large difference can be explained by the fact that shear fracture energy includes the energy required to create inclined tensile microcracks in the fracture process zone and the energy required to break the shear resistance provided by aggregate interlock. Therefore the crack propagation rate under this mixed-mode loading condition should be slower than a similarly stressed crack front under a pure mode I condition.

4.2.2 Adhesives

Sikadur 30 was used to adhere the laminate to the concrete. Sikadur 30 is a two-component, high-modulus, high-strength, structural epoxy paste. It conforms to ASTM C-881 and AASHTO M-235 specifications. The entire tensile strength is achieved after seven days of curing at room temperature. A .04 inch thick layer of Sikadur 30 was used to bond the laminate to the concrete along the length of the beam. Table 4.3 lists additional characteristics.

Typical Data for Sikadur 30	
Pot Life	30 min
Tensile Strength	3.6 ksi
Strain at Break	0.01
Young's Modulus	.65 Msi
Shear Strength (14 day)	3.6 ksi
Flexural Strength (14 day)	6.8 ksi

Table 4.3: Typical Data for Sikadur 30

Characteristics of FRP		
Characteristics	CFRP	GFRP
Tensile Strength	348 ksi	50 ksi
Young's Modulus	22.5 Msi	4.3 Msi
Strain at Break	0.019	0.024

Table 4.4: Characteristics of FRP

4.2.3 Laminates

Two different FRPs were used: GFRP and CFRP. The GFRP used was a grade G-10/FR-4, glass fibers embedded in an epoxy matrix. The CFRP used was Sika Carbodur, a pultruded CFRP with Toray T700 fibers in a graphite matrix. The fiber content in the CFRP is around 70%. The thickness of both laminates is roughly .047 inches. The laminates were cut to size using heavy-duty shears and cleaned with acetone. Other mechanical properties are shown in Table 4.4. Figure 4.3 shows the stress-strain relationships for the FRPs. The stress-strain behavior is essentially linear until the ultimate stress is achieved. At that point, the FRP yields at the ultimate strength until the laminate ruptures at the ultimate strain. Some of the properties were not available from the manufacturer and were calculated from small-scale experiments.

Stress in
ksi
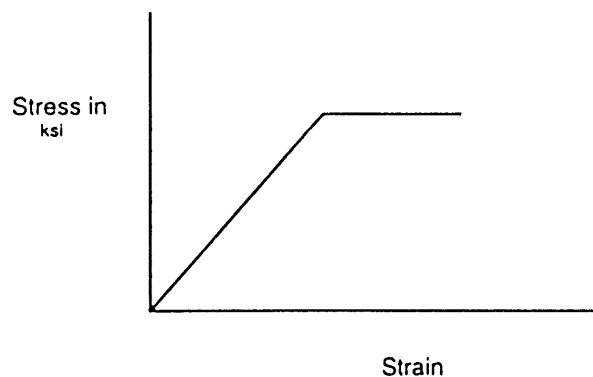
Strain

Figure 4.3: Stress-Strain Behavior of FRPs

4.3 Load Capacity of Specimens

As discussed, the unretrofitted specimens were designed to fail in tensile steel yielding. The CFRP and GFRP retrofitted beams were projected to fail by shear failure and laminate rupture, respectively. This section shows the load capacity calculations for different modes of failure.

Shear Failure for All Beams:

Total Shear Strength: $\qquad V_{max} = V_s + V_c$

Concrete Shear Strength: $\qquad V_c = 2b \cdot d\sqrt{f'_c} = 2(3.8)(4)\sqrt{5100} = 2.17 \text{kips}$

Steel Shear Strength: $\qquad V_s = \dfrac{A_s \cdot f_y \cdot d}{s} = 4.83 \text{kips}$

Total Shear Strength: $\qquad V_{max} = 7.0 \text{ kips}$

Total Load Resistance: $\qquad P_{max} = 2V_{max} = 14 \text{ kips}$

Since the shear reinforcement for all the beams is the same, the shear resistance should be the same for all beams, regardless of the amount of flexural retrofitting.

Flexural Failure of Unretrofitted Beams:

Steel Ratio: $\qquad \rho = A_s / bd = .0145$

Balanced Steel Ratio: $\qquad \rho_b = .85\beta_1 \dfrac{f'_c}{f_y}\left(\dfrac{87,000}{87,000 + f_y}\right) = .0342$

$\qquad\qquad\qquad\qquad \rho < \rho_b \qquad$ ∴ Beam will fail via tensile steel yield

Compressive Block: $\qquad a = \dfrac{\rho \cdot f_y \cdot d}{.85f'_c} = .76"\qquad$ Ignoring compression steel

Moment Resistance: $\qquad M_n = A_s f_y(d - \frac{a}{2}) = 45 \text{k} \cdot \text{in}$

Maximum Load Resistance: $\quad P_{max} = 6M_{max} = 7.52 \text{ kips}\qquad$ ∴ Flexural strength controls

Unretrofitted beams will fail via tensile steel yield.

Flexural Failure of GFRP Retrofitted Beams:

Steel Ratio: $\rho_{steel} = A_s / bd = .0145$

GFRP Ratio: $\rho_{laminate} = A_l / bd = .0032$

Balanced Steel Ratio: $\rho_{bsteel} = .85\beta_1 \dfrac{f'_c}{f_y}\left(\dfrac{87,000}{87,000 + f_y}\right) = .0342$

Balanced GFRP Ratio: $\rho_{bla\,minate} = .85\beta_1 \dfrac{f'_c}{f_y}\left(\dfrac{87,000}{87,000 + f_l}\right) = .0253$

Total Reinforcement Ratio: $\dfrac{\rho_{steel}}{\rho_{bsteel}} + \dfrac{\rho_{la\,minate}}{\rho_{bla\,minate}} = .574 < 1$ $\quad\therefore$ Beam will fail via steel yield

Compressive Block: $a = \dfrac{A_s \cdot f_y + A_l \cdot f_l}{.85f'_c} = .927"$ $\quad$ Ignoring compression steel

Moment Resistance: $M_n = A_s f_y (d - \frac{a}{2}) + A_l f_l (h - \frac{a}{2}) = 55.6 k \cdot in$

Maximum Load Resistance: $P_{max} = 6M_{max} = 9.3$ kips $\quad \therefore$ Flexural strength controls

GFRP retrofitted beams will fail via laminate rupture.
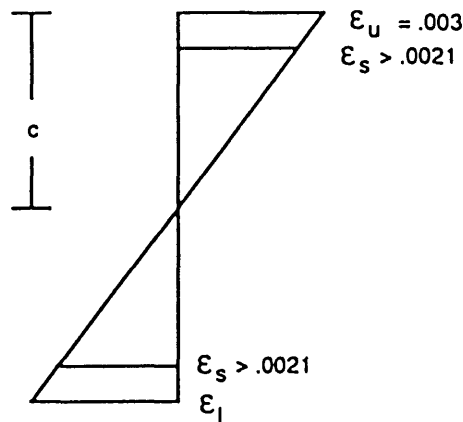
Figure 4.4: Strain Distribution at Failure for CFRP Retrofitted Beam

Flexural Failure of CFRP Retrofitted Beams:

Steel Ratio: $\rho_{steel} = A_s / bd = .0145$

CFRP Ratio: $\rho_{la\,minate} = A_l / bd = .0032$

Balanced Steel Ratio:	$\rho_{bsteel} = .85\beta_1 \dfrac{f'_c}{f_y}\left(\dfrac{87,000}{87,000 + f_y}\right) = .0342$	

Balanced CFRP Ratio: $\rho_{bla\,min\,ate} = .85\beta_1 \dfrac{f'_c}{f_y}\left(\dfrac{87,000}{87,000 + f_1}\right) = .00199$

Total Reinforcement Ratio: $\dfrac{\rho_{la\,min\,ate}}{\rho_{bla\,min\,ate}} = 1.61 > 1$ $\therefore$ Beam will fail via concrete crushing

Compressive Forces: $C = C_{steel} + C_{concrete} = A_s f_y + .85\beta_1 \cdot f'_c \cdot b \cdot c$

Tensile Forces: $T = T_{steel} + T_{la\,min\,ate} = A_s f_y + A_1 f_1$

Equating Forces: $c = .99"$

Compressive Block: $a = .80(c) = .79"$ Ignoring compression steel

Moment Resistance: $M_n = A_s f_y (d - \raise.5ex\hbox{a}/\!\lower.25ex\hbox{2}) + A_1 f_1 (h - \raise.5ex\hbox{a}/\!\lower.25ex\hbox{2}) = 101.3k \cdot in$

Maximum Load Resistance: $P_{max} = 6M_{max} = 16.9$ kips $\therefore$ Shear strength controls

CFRP retrofitted beams will fail via concrete shearing.

	Theoretical Behavior	
Beam Type	Failure Load	Mode of Failure
Unlaminated	7.5 kips	Steel Yield
GFRP Laminated	9.3 kips	GFRP Rupture
CFRP Laminated	14 kips	Shear Failure

Table 4.5: Theoretical Load Capacity of Unretrofitted and FRP Retrofitted Specimen

Table 4.5 summarizes the theoretical behavior of FRP retrofitted beams. As shown in the figure, the unlaminated beam, GFRP retrofitted beam, and CFRP retrofitted beam were predicted to fail via steel yield, GFRP rupture, and shear failure, respectively. However, these predictions assume that laminate peel-off failure will not occur at lower loads.

4.4 Experimental Set-up and Method

The 30 beams were investigated for maximum load capacity, mode of failure under cyclic and static loading, behavior of laminate, and fatigue characteristics. Beams were tested in an MTS loading machine (110 kip capacity) driven by an Instron control unit. A load cell on the MTS machine measured load. A deflection gauge measured the crosshead displacement which was a measure of the average deflection at the two inner loading points. Figure 4.5 shows a picture of the experimental set-up on the loading machine.
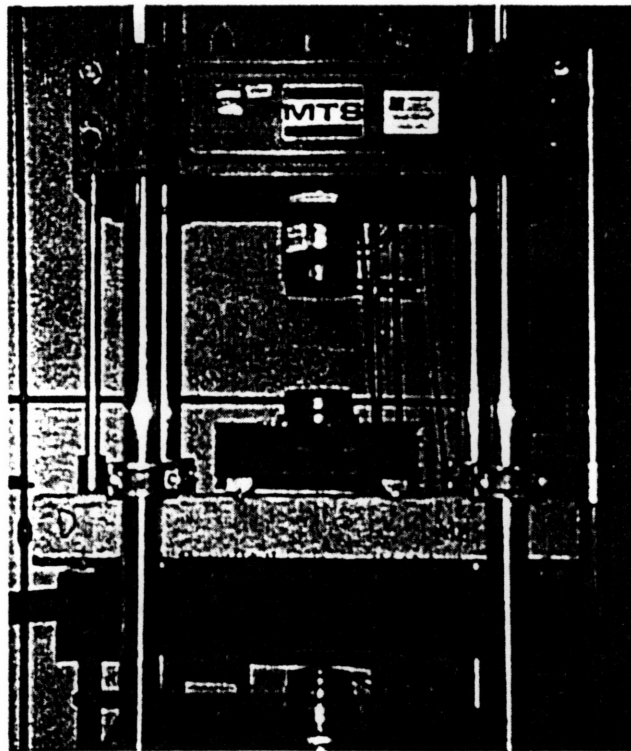
Figure 4.5: Experimental Set-Up

The delamination of the FRP laminate was monitored in three ways: a sharp change in beam stiffness, auditory detection, and visual detection. Delamination location and delamination growth will be measured visually. As discussed in Section 2.4.1, while the estimation of crack length using visual detection will include errors, as long as the error is consistent, the crack growth measurement will not sustain excessive estimation

errors. At first, crack length estimation was attempted using beam stiffness calibration. However, due to beam damage other than crack growth, it was difficult to relate beam stiffness to crack length.

4.4.1 Bonding FRP to Concrete

In order to provide an adequate bonding surface, the RC beam was cleaned with compressed air in order to remove dust, laitance, and other foreign particles. In some cases, the beam was sandblasted to create a rough surface. This allowed the epoxy to interlock with the aggregate for superior bonding. The laminates were wiped clean with acetone.

The freshly mixed epoxy was then placed onto the concrete with a spatula. Next, the laminate was positioned on the epoxy and pressed into the resin until the adhesive was forced out on both sides. The resulting epoxy thickness was roughly .04 inches. The epoxy was air dried for seven days at room temperature before the retrofitted beam was tested in static or cyclic loading.

Initial delaminations were fabricated at both ends of the beam specimen. The laminate was clamped to the RC beam at given initial delamination locations, dc. The ends of the laminates were then pried off the beams and stripped in a pure mode I fashion to the clamping point. When stripped off the beam, the FRP also removed a thin layer of concrete. This layer of concrete was similar to the laminate in thickness (.047 to .141 inches thick). Thus initial delaminations of length dc were manufactured on both ends of the beam, initiating a crack in the concrete.

4.4.2 Discussion of Test Method

This research program investigates the effect of two parameters for static loading:

1) Laminate Stiffness: glass fiber and carbon fiber

2) Surface Roughness: smooth (unsandblasted) and sandblasted

This will yield 4 mutations of this test. Table 4.5 summarizes the various testing parameters. The cyclic load test program only includes CFRP retrofitted beams, but does study one parameter, namely surface roughness.

Type	Composite	Concrete Surface
1	GFRP	Cleaned
2	CFRP	Cleaned
3	GFRP	Sandblasted
4	CFRP	Sandblasted

Table 4.6: Summary of Testing Parameters

The characteristics of the GFRP and CFRP were discussed in Section 4.2.3. It is hypothesized, however, that only two characteristics of FRP will significantly affect peel-off behavior: laminate roughness and stiffness. Laminate roughness will affect the strength of the adhesive bond between the FRP and the epoxy. A higher laminate stiffness will induce higher local stresses at the concrete-laminate interface. Thus, it is suggested that a higher laminate stiffness will induce peel-off at lower loads.

Surface roughness may also have an important effect on delamination load. A rough surface, as provided by sandblasting, will improve the adhesive bond between the laminate and the concrete. Thus it is theorized that sandblasting will increase the delamination load and delamination propagation resistance.

4.4.2.1 Static Load Testing

Sixteen beam types will be prepared for static testing in order to form the fast fracture interaction curve. Table 4.7 summarizes the characteristics of these sixteen beams:

Type	Composite	Concrete Surface	Delamination Location (in)
1	GFRP	Sandblasted	6
2	GFRP	Sandblasted	9
3	GFRP	Sandblasted	12
4	GFRP	Sandblasted	14
5	GFRP	Cleaned	6
6	GFRP	Cleaned	9
7	GFRP	Cleaned	12
8	GFRP	Cleaned	14
9	CFRP	Sandblasted	6
10	CFRP	Sandblasted	9
11	CFRP	Sandblasted	12
12	CFRP	Sandblasted	14
13	CFRP	Cleaned	6
14	CFRP	Cleaned	9
15	CFRP	Cleaned	12
16	CFRP	Cleaned	14

Table 4.7: Summary of Static Tests

As shown in the table, the four beam types outlined in Table 4.6 are tested with four different initial delamination locations. These initial delamination locations are set at 6, 9, 12, and 14 inches. Using the delamination loads for each beam configuration, any point on the fast fracture interaction curve can be extrapolated or interpolated.

The beam will be loaded at a rate of .05 in/min at the two loading points. The fast fracture of the laminate will be evident by a sharp drop in beam stiffness (or load capacity), but will be confirmed with auditory and visual detection. The mode of beam failure will also be recorded in order to determine a relationship between delamination location and beam failure mode.

4.4.2.2 Cyclic Load Testing

Only CFRP post-reinforced beams will be tested under cyclic loading, but surface preparation will be varied. The load will oscillate at ΔP, between a maximum loading (between 50-90% of beam fast fracture resistance capacity) and a minimum loading (unloaded). The beam will be sinusoidally loaded at a frequency at 1 Hz.

The deflection, which is a function of crack length, will be continually monitored,

in order to monitor the degradation of beam stiffness due to crack propagation and other beam damage. By monitoring beam stiffness, crack growth can be verified, as delaminating beams will show more stiffness degradation. Additionally, after every test period, usually 1000 cycles of loading, the new delamination location will be measured visually in order to estimate delamination growth. The cyclic load range may also be reset in order to promote or retard the crack propagation rate. This process will continue until complete failure of the beam or the concrete-laminate bond.

EXPERIMENTAL RESULTS AND ANALYSIS

5.1 Introduction

This chapter presents the experimental data and analyzes the results. Data yielded the sought after failure interaction curve and the Paris Power constants, which in turn allow a comparison and characterization of concrete-laminate interface toughness and fatigue resistance. These results also provided insight into the effects of different laminate types and surface preparation on the toughness and fatigue resistance of the concrete-laminate interface. Additionally, the methodology for evaluating the fatigue properties, as discussed in the previous chapter, proved to be effective.

5.2 Modes of Concrete-Laminate Interface Failure

All the retrofitted beams with initial delaminations tested under static and cyclic loading failed via delamination failure. Since initial delaminations would not allow the necessary development length, the length of laminate necessary for sufficient anchorage, proper laminate bond strength was not achieved. However, delamination failures differed significantly. Bond failures can be divided into three major categories:

1) Delamination at the laminate-concrete layer through a thin layer of concrete, the adhesive-concrete interface, or the adhesive-laminate interface

(Delamination or DLM)

2) Debonding of the concrete from the tension steel (Debonding or DBD)

3) Propagation of the delamination into the concrete as a shear crack (Delam/Shear or DLS) or flexural crack (Delam/Flex or DLF)

Other types of failures, such as laminate rupture, were not observed. The modes of interface failure are depicted in Figure 5.1:
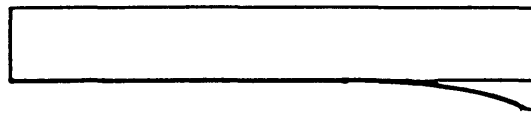
a) Delamination at the laminate-concrete interface through a thin layer of concrete
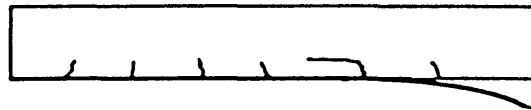
b) Debonding of the concrete from the tension steel
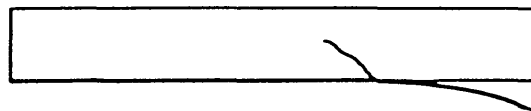
c) Propagation of the delamination into the concrete as a shear crack

Figure 5.1: Various modes of delamination failure

The third delamination mode, DLS or DLF, is a hybrid of delamination at the concrete-laminate interface and shear or flexural cracking. However, it should be categorized as a specific delamination mode because it has its own particular characteristics. The crack initiates as a delamination at the concrete-laminate interface, however, this crack deflects into a flexural or shear crack. It is unknown whether this propagation deflection is a result of an aggregate in the crack path, an existing shear or flexural crack, or the particular stress characteristics at the point of crack deflection. All of these delamination modes were initiated with artificially manufactured delaminations,

as discussed in Section 4.4.1. Initially, these delaminations manufactured through the concrete propagated through this thin concrete layer (.047 to .141 inches thick). However, as the cracks continued to propagate, the cracks would remain in this thin layer of concrete, would continue as debonding cracks at the concrete-steel interface (.7 inch thick concrete layer), or would continue into shear or flexural cracks. Figure 5.2 illustrates these three cracking patterns in the interfacial region. Cracking patterns indicated that all interface failures initiated at the concrete-laminate interface where the initial delamination was artificially manufactured. Thus, at some point during interfacial failure, DLM occurred and propagated to compromise beam integrity.
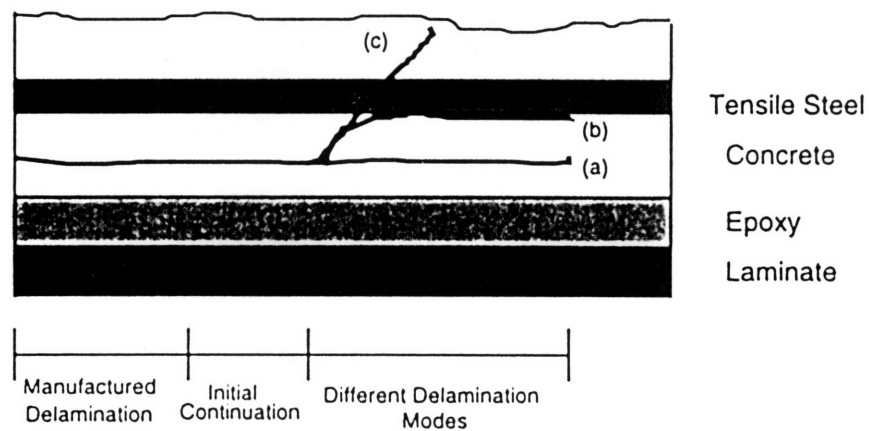
a) Delamination in Thin Layer of Concrete, b) Debonding at Steel-Concrete Interface,
c) Delamination into a Shear Crack

Figure 5.2: Cracking Patterns of Various Delamination Modes

The major stress on the concrete crack is the tensile stress provided by the FRP laminate. This stress is parallel to the DBD cracks and the DLM cracks suggesting that these cracks not only initiate, but also propagate under mixed mode stress conditions, if not pure Mode II stress conditions. This mixed mode condition is considered further in Section 5.4.1.

While these three failure modes are notably different, specific load configurations did not dictate the mode of failure. That is, two beams prepared and tested in the same

fashion could result in different delamination failure modes. All of the cracks were artificially manufactured in the concrete layer directly above the laminate and initially propagated along this layer, but in some cases deviated onto different crack paths. However, most of the delaminations occurred in the concrete in one fashion or another implying that it is the concrete fracture toughness, not the concrete-laminate interface fracture toughness, which resists delamination propagation. Thus, while laminate type or surface preparation may affect delamination resistance, it is the concrete fracture toughness which is seemingly the most significant parameter.

Beam Type	Theoretical Results		Experimental Results	
	Failure Load	Mode of Failure	Failure Load	Mode of Failure
Unlaminated	7.5 kips	Steel Yield	9.7 kips	Steel Yield
GFRP Laminated	9.3 kips	GFRP Rupture	11.1 kips	GFRP Rupture
CFRP Laminated	14 kips	Shear Failure	11.0 kips	CFRP Peel-off

Table 5.1: Behavior of Unretrofitted and FRP Retrofitted Specimens

5.3 Analysis of Static Load Testing

28 beams were tested under static loading: one control beam, two fully laminated beams, and 25 retrofitted beams with initial delaminations. Unretrofitted and fully laminated CFRP and GFRP retrofitted beams were tested in monotonic loading to failure to ascertain the accuracy of the predicted failure modes and failure loads. Failure loads were predicted with reasonable accuracy for the unretrofitted and GFRP retrofitted beams. However, the CFRP retrofitted beam failed via laminate peel-off prior to achieving its theoretical maximum load capacity. As shown, laminate peel-off prevented the CFRP retrofitted beam from attaining its maximum theoretical load capacity. Table 5.1 summarizes the theoretical predictions and experimental results of monotonic load tests.

Table 5.2 displays the delamination loads of the static load tests. (More detailed results are presented in the Appendix, Section A.1.) Some beam configurations were

tested more than once. Thus, the results given are average delamination loads for given beam types. Data was somewhat variable (see Section A.1), with individual data mostly varying less than 10% from the average delamination load. Maximum variation from average delamination loads was 18.5%; thus, no data was excluded. This table also displays how the average delamination load approaches a constant value after the delamination location, the distance from the delamination to the support, is greater than twelve inches, the distance between the support and the nearest load. This is to be expected: from 12-24 inches, the beam is under constant shear and moment suggesting that any delamination tip in this region would experience similar stress conditions. The table also reveals how delamination load decreases for larger initial delamination locations.

Type	Composite	Concrete Surface	Delam Location (in)	Avg. Delam Load (kips)
1	GFRP	Sandblasted	6	9.85
2	GFRP	Sandblasted	9	9.45
3	GFRP	Sandblasted	12	9.33
4	GFRP	Sandblasted	14	9.36
5	GFRP	Cleaned	6	8.67
6	GFRP	Cleaned	9	8.34
7	GFRP	Cleaned	12	8
8	GFRP	Cleaned	14	8.17
9	CFRP	Sandblasted	6	10.32
10	CFRP	Sandblasted	9	10.1
11	CFRP	Sandblasted	12	9.03
12	CFRP	Sandblasted	14	9.03
13	CFRP	Cleaned	6	9.9
14	CFRP	Cleaned	9	9.36
15	CFRP	Cleaned	12	8.9
16	CFRP	Cleaned	14	9.01

Table 5.2: Results of Static Load Tests

5.3.1 Determination of the Delamination Load

Figure 5.3 shows typical results for statically loaded RC beams, sandblasted and retrofitted with FRP. The load-deflection curves show the increase in beam deflection as

the load is increased. Between 8 and 10 kips, the steel begins to yield, affecting the stiffness of the beam. At this yield point, the load-deflection curve begins to plateau.

Load-Deflection Behavior of GFRP Retrofitted Beams

a) Sandblasted RC Beams Retrofitted with GFRP

Load-Deflection Behavior of CFRP Retrofitted Beams
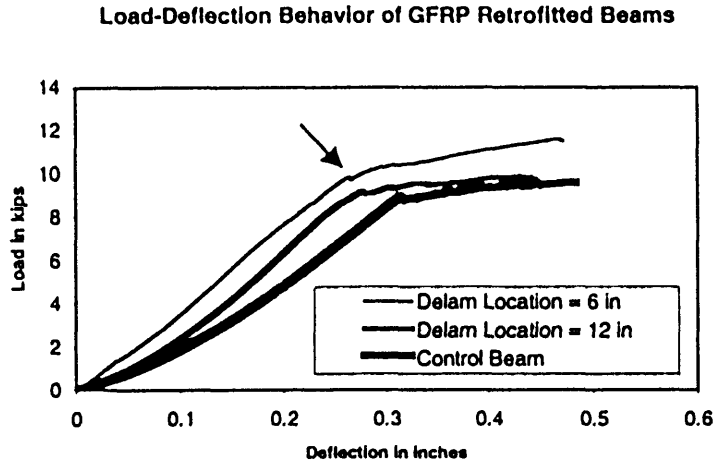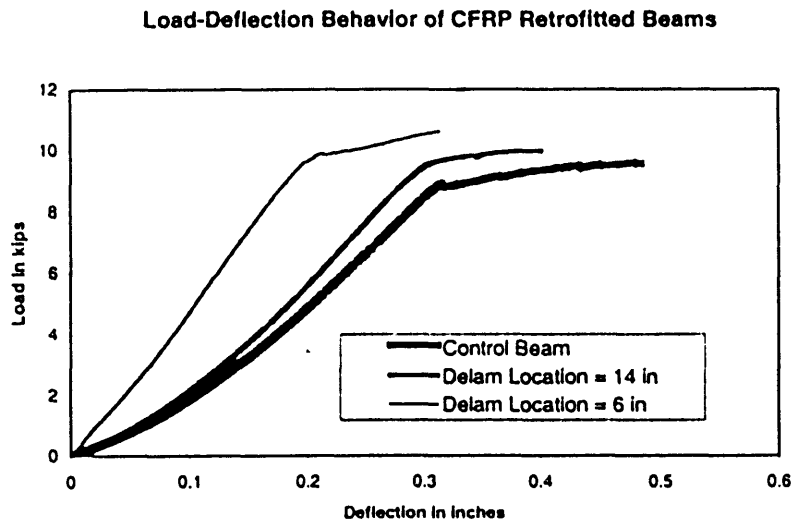
b) Sandblasted RC Beams Retrofitted with CFRP

Figure 5.3: Load –Deflection Curves for Statically Loaded Sandblasted Beams Retrofitted with FRP

The detection of delaminations during static testing was very difficult, if not infeasible, using beam stiffness monitoring. As shown in the results, there is often no sharp drop in beam stiffness with FRP delamination. The black arrow in Figure 5.3(b) demarcates a slight drop in stiffness associated with an unstable delamination, but these slight stiffness drops are not detectable in the other load-deflection curves shown. In most cases these curves are smooth despite the occurrence of unstable delamination propagation. However, upon visual inspection of the beams during loading, delamination was easily detected, yielding the associated delamination load, the load at which the FRP peels-off from the beam. Therefore, load-deflection data was used only to confirm visual detection results when stiffness results were useful.

The load-deflection diagrams do show the correlation between delamination location and beam stiffness. As the anchorage length increases, the beam stiffness increases too. Clearly, as the anchorage length increases, the beam's overall stiffness increases, improving flexural strength at the ends of the beam. This increase in the beam's stiffness reduced deflections. Also shown in these charts is that in some cases, the retrofitted beams ultimate strength converges to that of the control beam (e.g. Figure 5.3(b) Delam Location = 12 in). This indicates that complete or nearly complete failure of the interface has occurred as beam behavior is similar to that of an unretrofitted beam. In other cases, the ultimate beam strength diverges from that of the control beam (e.g. Figure 5.3(b) Delam Location = 6 in). This indicates that while there was propagation of the delamination, the failure of the interface was incomplete as the laminate still contributed load carrying capacity.

5.3.2 Static Load Testing of GFRP Retrofitted Beams

Based on the data given in Table 5.2, failure interaction curves were constructed. Failure interaction curves were constructed using average values. A linear trendline will predict values in the 0-12 inch delamination region. Using the assumption that the delamination load remains constant in the 12-24 inch region, a constant linear trendline, set at the average of the delamination load values for delamination locations of 12 and 14

inches, models the interaction curve in the 12-14 inch delamination region. This produces the failure interaction curves shown in Figure 5.4.

The curve is comprised of two sets of data: the average delamination loads for sandblasted beams and the average delamination loads for smooth beams. These average values are represented by triangles or circles. The interpolated failure interaction curve is represented by a dashed or solid line.

Failure Interaction Curve for Beams Post-Reinforced with GFRP

Figure 5.4: Failure Interaction Curves for Beams Post-Reinforced with GFRP Laminates

Figure 5.4 shows the failure interaction curve for a GFRP retrofitted beam. The chart shows how the delamination load decreases as the delamination location increases. Also, the delamination loads of sandblasted beams are consistently lower than delamination loads of smooth beams. This demonstrates that the concrete-laminate bond is weaker if the beam is not sandblasted. Sandblasting allows the epoxy to interlock with the aggregate. Thus, surface preparation is a way to improve delamination resistance.

More importantly, this data shows how delamination location is important for the delamination resistance of GFRP. When fully laminated, the GFRP laminated beam failed by laminate rupture, achieving its maximum flexural strength. However, when initial delaminations are created, these beams fail via delamination. Thus, anchorage length will improve the delamination resistance of these beams.

**Failure Interaction Curve for Beams
Post-reinforced with CFRP**
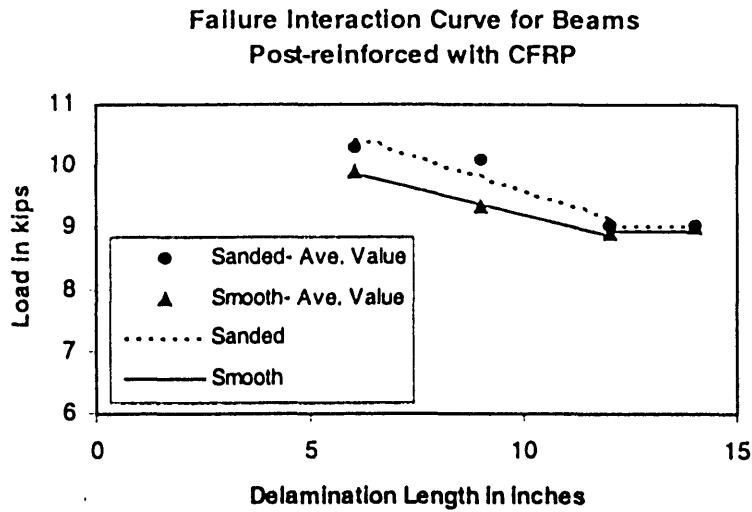
Figure 5.5: Failure Interaction Curves for Beams Post-Reinforced with CFRP Laminates

5.3.3 Static Load Testing of CFRP Retrofitted Beams

Figure 5.5 displays the failure interaction curve for CFRP retrofitted RC beams. Again, the sandblasted beams have higher delamination loads than smooth beams. Additionally, the delamination location affects the delamination resistance of the CFRP retrofitted beams. As the delamination location is increased, the delamination load decreases.

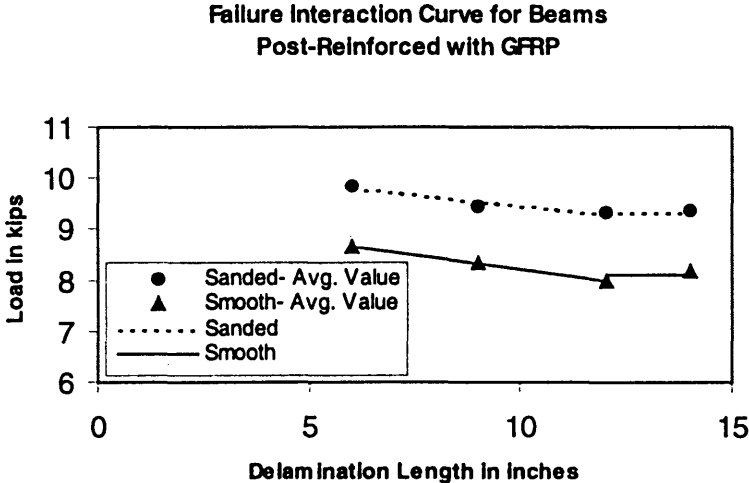**Failure Interaction Curve for Beams
Post-Reinforced with FRP**
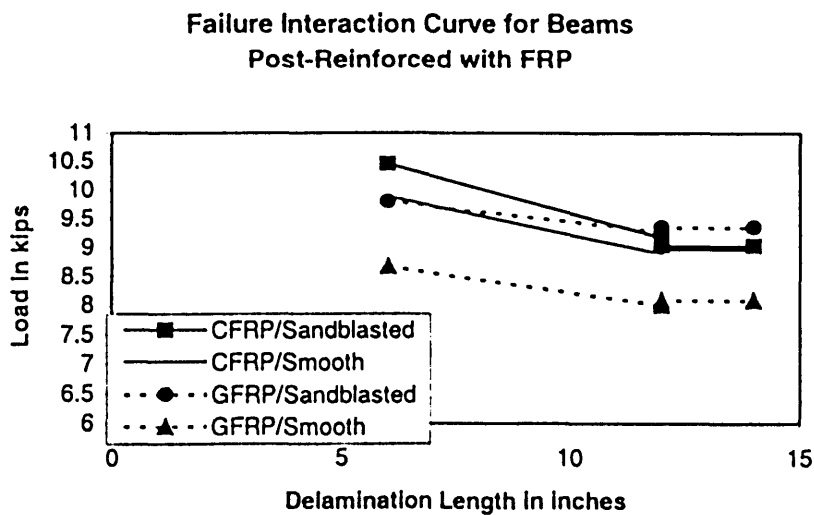
Figure 5.6: Failure Interaction Curves for Beams Post-Reinforced with FRP Laminates

Figure 5.6 consolidates the failure interaction curves onto one chart. From this chart, inherent differences between CFRP retrofitted beams and GFRP retrofitted beams are apparent. This chart shows how CFRP retrofitted beams are more delamination location sensitive. It is unclear from these tests which laminate has better bonding properties. It seems, however, that CFRP laminates have slightly better bonding performance.

While these interaction curves offer insight into the nature of post-reinforcement under static loading, the main purpose of these interaction curves is to form the framework for solving the Paris Power Law constants for the concrete-laminate interface. These constants should provide a basis for quantifying the long-term delamination resistance of the concrete-laminate interface.

5.4 Analysis of Cyclic Load Testing

Five beams were tested for cyclic loading: one control beam and four CFRP retrofitted beams. No GFRP retrofitted beams were tested under cyclic loading. Each beam sustained approximately 30 test periods, each test period usually consisting of 1000-1200 load cycles. The delamination propagation modes under cyclic loading are similar to the bond failure modes under static loading: failure of the concrete-laminate bond, debonding of the concrete from the tension steel, and propagation of the delamination into the concrete as a flexural or shear crack. All three modes involve the propagation of a crack through concrete which ultimately compromises the concrete-CFRP laminate interfacial bond.

Only delaminations at the concrete-laminate layer were measured. This is because only their initial and final states were easily related to the static failure interaction curves. That is, since initial delaminations were initiated at this concrete-laminate layer, only a propagation at this layer could be justifiably related to the failure interaction curve created by static tests. However, as stated, there were three possible crack propagation modes. In fact, delamination through the concrete along concrete-laminate interface, delamination mode DLM, only occurred for 15-20% of all test periods. Crack

propagation usually occurred as a delamination that continued into a flexural or shear crack, delamination mode DLF or DLS, respectively. Accordingly, only a small percentage of cyclic load tests were included in this analysis, as data for test cycles that did not manifest as DLMs was excluded. Due to the exclusion of much of the data, particularly test cycles that did not propagate delaminations as DLMs, the crack propagation data may overestimate the propensity of the interface to delaminate. On the other hand, some of the delaminations may not have been detected by visual inspection, a deficiency which may have resulted in the underestimation of delamination growth. This shortcoming is addressed in Section 6.3.

Beam Stiffness Degradation
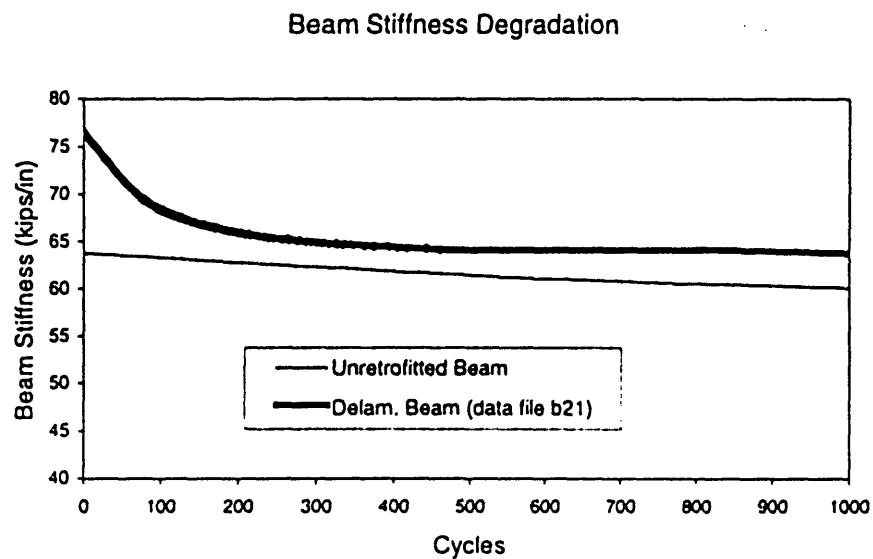
Figure 5.7: Loss of Beam Stiffness under Cyclic Loading

Unfortunately, stiffness calibration was not a viable delamination monitoring method. As shown in Figure 5.7, a cyclically loaded control beam loses stiffness as each load cycle progressively damages the beam. Hence, stiffness calibration for delamination location was extremely difficult, if not infeasible, since beam stiffness decreased with beam damage unassociated with delamination growth. Since stiffness calibration was not a viable method for determining delamination location, delamination location and delamination growth was measured visually at the end of each test cycle.

In addition, Figure 5.7 shows how delamination also induces a decline in beam stiffness. Fatigued in the same cyclic load range (0-6 kips), the delaminating beam shows

76

a more dramatic loss in stiffness. In this chart, beam stiffness represents the maximum load divided by the maximum average deflection measured at the midspan load points.

Fatigue Curve- CFRP/Sandblasted

$$y = 0.0049x^{4.5108}$$
$$R^2 = 0.2591$$

Ratio of Cyclic Load Range to Delamination Load
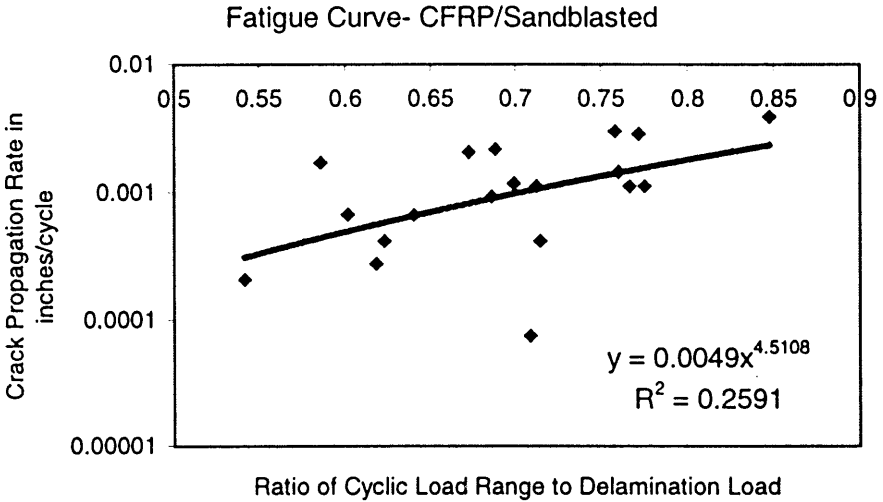
a) Fatigue Curve for Sandblasted Beams Post-Reinforced with CFRP

Fatigue Curve- CFRP/Smooth

$$y = 0.0046x^{5.8371}$$
$$R^2 = 0.2595$$

Ratio of Cyclic Load Range to Delamination Load
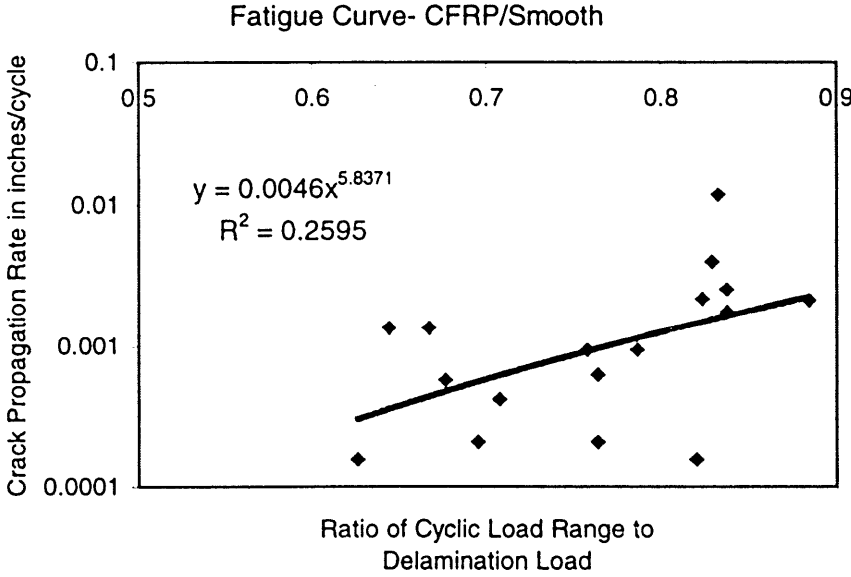
b) Fatigue Curve for Smooth Beams Post-Reinforced with CFRP

Figure 5.8: Fatigue Curves for Sandblasted and Smooth Beams Post-reinforced with CFRP

5.4.1 Fatigue Curves

Figure 5.8 shows the fatigue curve, plotted on a log-linear graph, for CFRP reinforced beams with either sandblasted or smooth concrete surfaces. (More detailed data is presented in the Appendix, Section A.2.) The crack propagation rate, crack growth per cycle, was taken to be the average crack propagation rate over a particular testing period (usually 1000 load cycles). This will offer only an estimation of crack propagation rate. The figure shows delamination growth plotted against the ratio of cyclic load ratio to delamination load: Here the delamination load was taken to be the average delamination load over a particular testing period. As postulated in the analysis, this is the same as the ratio of cyclic stress intensity to the stress intensity at bond failure for a given delamination location.

Suggested Paris Power Law constants are shown on the figures along with R^2, the correlation factor. The m factor, that is the Paris exponent, for both the sandblasted and smooth beams is in the 4-6 range. This m factor is comparable to the m factors of metals which have m factors between 3-5. The m factor for concrete under pure tension (mode I) is around 10 [10]. This suggests that concrete in this configuration is under a mixed mode stress configuration. Hence, the crack propagation rate is relatively insensitive to the stress intensity at the delamination tip. As shown on the curves, the A and m Paris factors are slightly higher for smooth beams. This suggests that the fatigue resistance of sandblasted beams is superior. This is due to the improved bond performance.

As discussed, the fracture toughness of concrete in tension was estimated to be 1.04 ksi·in$^{1/2}$ (1.14 MPa·m$^{1/2}$ in metric units). This is taken to be a rough estimation of the mixed mode fracture toughness. Using Equation 2.8, the Paris constant for sandblasted beams, A, can be estimated at .00411 (for da/dN in inches per cycle and ΔK in ksi·in$^{1/2}$). In metric units, this value is $6.9*10^{-5}$ (for da/dN in meters and ΔK in MPa·m$^{1/2}$). This is very high, even for concrete. However, substituting the correct stress intensity, which should be significantly higher due to mode II effects, will yield a Paris constant closer to standard Paris constant values. Thus, although the crack propagation rate is relatively insensitive to stress intensity, it still propagates at a significantly high rate. The long-term stability under high-intensity load cycles is suspect. However, the magnitude of the

delaminations (ranging as high as 4 inches per 1000 cycles), implies that the interface can withstand short-term, high intensity loading (as from an earthquake).

Finally, the correlation factor, R^2, is somewhat low. This is due to the high variability in concrete and the uncertainty that is inherent in fatigue testing. Thus, these suggested Paris Power Law constants should be used merely to gain an understanding into the behavior of this interface under high-intensity, cyclic loading. Any use of this data for design purposes, as for any design of concrete structures or long-term loading, should include highly conservative safety factors.

5.5 Summary

The experimental program and results presented here offer a greater understanding into the concrete laminate interface. The failure interaction curves and fatigue curves yielded insight into the fracture properties and the fatigue delamination properties of the interface, as well as insight into the benefits yielded by variations in construction methods. Additionally, the failure interaction curves showed the effect of delamination location on the delamination resistance of the system.

Cyclic and static testing showed three different modes of delamination failure. However, all the delamination modes initiated and at some point propagated in a thin layer of concrete above the laminate. This showed that concrete fracture toughness was a major controlling parameter in delamination resistance.

Failure interaction curves based on delamination loads at given delamination locations revealed the importance of sandblasting to the delamination resistance of the system. Additionally, the differences in FRP stiffness were shown to affect the sensitivity to delamination location. Most importantly, as the delamination location increased, delamination load decreased. This revealed the importance of anchorage length to the delamination resistance of the system.

Finally, CFRP retrofitted beams were tested under cyclic loading. Tests showed that FRP delamination can propagate in a stable manner at cyclic loads below the

delamination load. Additionally the overall rate of delamination in these tests was high suggesting that the interface is vulnerable to long-term, high-intensity loading.

However, for each question answered, a new one arises. Additionally, the shortcomings of this program, particularly regarding delamination location detection, are evident as one reviews the results. Thus, the results presented here offer suggestions further research.

CONCLUSIONS

6.1 Summary

As the use of FRP for the post-reinforcement of concrete structures becomes increasingly widespread, an understanding of the cyclic load resistance, as well as the high-intensity load resistance of the post-reinforced system will become essential. As shown in previous research, peel-off failure, or failure of the concrete-laminate interface, is a common mode of failure. Unfortunately, little is known about the interface. This study has provided some fundamental knowledge concerning the fatigue properties, as well as the fracture properties, of the concrete-laminate interface.

A three-foot long RC beam specimen was constructed to test the properties of the concrete-laminate interface. These specimens were retrofitted with FRPs, varying FRP type (GFRP or CFRP) and concrete surface roughness (sandblasted and smooth). Peel-off at the interface was initiated to induce peel-off failure.

First, beams were tested under static loads to test the fast-fracture properties of the interface. By varying initial delamination location, the beams were tested to find the load at delamination failure. Using this data, failure interaction curves were constructed not only to form a comparative basis for the construction variations, but to construct a framework for analyzing the behavior under cyclic loading.

The beams were then tested for cyclic load behavior. Delaminations at the interface were propagated at loads lower than the delamination loads. Delamination growth as a function of cyclic load range was recorded. Using this data, fatigue curves were constructed in order to obtain Paris Power Law constants.

6.2 Conclusions

The static and cyclic load test results obtained in this research program yield a deeper understanding of the behavior of the delamination resistance of the concrete-laminate interface. This understanding creates suggestions for improvements in the use of this post-reinforcement technology, as well as guidelines for the use and design of post-reinforcement.

First, static load tests were conducted on fully laminated beams to compare the theoretical results with the actual results. It was shown that the control beam and the GFRP failed via their predicted failure modes: steel yield and GFRP rupture, respectively. However, the CFRP retrofitted beam did not fail by way of concrete shear as predicted. Instead, the system failed via laminate peel-off at an ultimate load well below the predicted ultimate load.

Next, static load tests were performed on laminated beams with initial delaminations. All these beams had failures of the concrete-laminate interface. All delaminations, manufactured at the interface, initially propagated along the interface through the concrete. Thus the fracture properties of the concrete is a significant factor in the peel-off failure of retrofitted beams.

The static load tests were used to construct failure interaction curves which revealed the influence of FRP stiffness and concrete surface preparation on the system's delamination resistance. It was shown that CFRP retrofitted beams were more sensitive to delamination location than GFRP retrofitted beams. Sandblasting also improved the delamination resistance of the concrete-laminate interface. Since the sandblasting allows the epoxy to interlock with the concrete's aggregates, the epoxy-concrete bond stability is improved. Additionally, the delamination resistance of the retrofitted system was sensitive to the location of the delamination location.

The cyclic load tests provided fatigue curves which plotted the delamination growth rate against the ratio of cyclic load range to delamination load. Delamination propagation occurred at load ranges lower than the delamination loads, showing the vulnerability of this interface to fatigue loading. From the fatigue curves Paris Power Law constants were estimated and compared to known Paris Power Law constants. The

m factor, the Paris exponent, is comparable to that of metals, low compared to that of concrete in pure tension. This shows that at high-intensity load levels the interfacial fatigue resistance is relatively insensitive to stress intensity. However, the A factor, the Paris constant, is very high. The crack propagation rate is usually severe. Thus the interface is vulnerable to long-term, high-intensity loading.

Both the static and cyclic results suggest that the delaminations, which are manifested as concrete cracks, are propagating under mode II or mixed mode conditions. Since the direction of the cracks in the concrete is parallel to the applied force, the tensile force from the laminate, it can be inferred that these cracks are propagating under mode II or mixed mode conditions. Cyclic tests also suggest mixed mode conditions exist at the crack front as the Paris Power Law constants differ significantly from concrete in pure tension.

6.3 Recommendations for Further Research

Recommendations for further research can be divided into two parts: ways to improve and extend this current research program, and novel suggestions for further research. Improvements in this research project include:

- Improvements in delamination growth measurement methods. Suggestions include nondestructive testing methods (ultrasound technology) and strain gauges on the laminate to detect where the laminate is unstressed.
- It was assumed that the delamination load of a statically loaded, pre-delaminated beam was the same as the delamination load of a cyclically loaded (and damaged) beam. Concrete research has shown how concrete fracture behavior differs before and after cyclic loading [19, 20]. Further tests would confirm or improve the accuracy of the Paris Power Law constants by ascertaining the exact difference between these two types of delamination loads. Thus any discrepancies between the behavior of statically loaded and cyclically loaded beams could be, at least in part, eradicated.

This experimental program also suggests ideas for further research:

- Similar delamination resistance tests should be performed using concrete of varying fracture toughness. These tests should confirm the assumption that concrete fracture toughness is a controlling factor for delamination resistance. This assumption indicates that post-reinforcement should only be applied to concrete beams with relatively high fracture toughness.

- As discussed in Section 3.4, Drory et al. suggest an equation for the fracture energy for the decohesion of residually stressed thin films from a substrate [33]. Since the delamination of a thin composite laminate from the concrete is similar to the decohesion of a thin film from a substrate, Drory's fracture energy equation can be applied to these post-reinforced beams. The fracture energy equation developed by Drory et al. requires a knowledge of the stress, σ, at the delamination tip. This stress, however, is difficult to calculate using simple beam theory. Further tests on these beams with initial delaminations placing strain gauges on the composite at the delamination tip will allow a numeric analysis (not an indirect analysis) of the fracture energy at this interface using a fracture mechanics approach.

- There are numerous factors which may affect the delamination resistance of the concrete-laminate bond. Therefore an investigation into these different factors may offer improvements into current application techniques:

  - Epoxy type
  - Laminate width
  - Various surface preparation techniques (i.e. pneumatic blasting)
  - Size effect

This research program has shown that the peel-off failure of laminates can occur well below the design failure of the post-reinforced beam. This failure can occur as a fast fracture or as a crack propagation under fatigue. This emphasizes the necessity for an

understanding of the fracture properties of this interface as peel-off failure may control post-reinforcement design and especially service life estimation. It is clear that further research is required for reliable post-reinforcement design.

REFERENCES

1. Saadatmanesh, H. and Ehsani, M. (1991), "RC Beams Strengthened with FRP plates II: Analysis and Parametric Study", *Journal of Structural Engineering*, 117(11), pp. 3434-3455.
2. Meier, U., (1995), "Strengthening of Structures Using Carbon Fibre/Epoxy Composites", *Construction and Building Materials*, 9(6), pp. 341-351.
3. Arduini, M., Nanni, A. (1997), "Behavior of Precracked RC Beams Strengthened with Carbon FRP Sheets", *Journal of Composites for Construction*, 1(2), pp. 63-70.
4. Chajes, M., et al. (1994), "Durability of Concrete Beams Externally Reinforced with Composite Fabrics", *Construction and Building Materials*, 9(3), 1995, pp. 141-148.
5. Inoue, S., et al. (1996), "Deformation Characteristics, Static and Fatigue Strengths of Reinforced Concrete Beams Strengthened with Carbon Fiber Reinforced plastic Plate", *Transactions of the Japan Concrete Institute* 18, 1996, pp.143-150.
6. Deuring, M. (1993), "Verstarken von Stahlbeton mit gespannten Faserverbundwerkstoffen", EMPA, Dubendorf.
7. Ashby, M., Jones, D. (1993), *Engineering Materials I*, Pergamon Press, Oxford, pp. 135.
8. Forsyth, P. (1961), "A Two-stage Process of Fatigue Growth", *Crack Propagation Symposium*, 1, pp.76-94.
9. Knott, J., Withey, P. (1993), *Worked Examples in Fracture Mechanics*, The Bourne Press, Bournemouth, pp.90.
10. Bazant, Z., Xu, K. (1991), "Size Effect in Fatigue Fracture of Concrete", *ACI Materials Journal*, 88(4), pp. 390-399.
11. Broek, D. (1986), *Elementary Engineering Fracture Mechanics*, Kluwer Academic Publishers, Dordrecht.
12. Broek, D. (1989), *The Practical Use of Fracture Mechanics*, Kluwer Academic Publishers, Dordrecht.
13. "Considerations for Design of Concrete Structures Subjected to Fatigue Loading", *Journal of the American Concrete Institute*, 71(3), pp. 97-121.
14. Broek, D., Schijve, J. (1966), "Fatigue Crack Growth: Effect of Sheet Thickness", *Aircraft Engineering*, 38(11), pp. 31-33.
15. Anderson, T. (1995), *Fracture Mechanics Fundamentals and Applications*, CRC Press, Boca Raton, pp. 354-357.
16. James, C., Schwenk, E. (1971), "Fatigue Crack Growth 304 Stainless Steel at Elevated Temperature", *Met. Trans*, 2, pp.491-503.
17. Nibkin, K., and Webster, G. (1988), "Prediction of Crack Growth under Creep-Fatigue Loading Conditions", *Low Cycle Fatigue*, ASTM STP 942, edited by Solomon, H., et al., American Society for Testing and Materials, Philadelphia, pp. 281-292.
18. Schijve, J., Broek, D. (1962), "Crack Propagation Tests Based on a Gust Spectrum with Variable Amplitude Loading", *Aircraft Engineering*, 34, pp. 314-316.

19. Perdikaris, P., Calomino, A., Chudnovsky, A. (1986), "Effect of Fatigue on Fracture Toughness", *Journal of Engineering Mechanics, ASCE*, 112(8), pp. 776-790.

20. Swartz, S., Huang, C., Hu, K. (1982), "Crack Growth and Fracture in Plain Concrete- Static versus Fatigue Loading" in *Fatigue of Concrete Structures*, ed. Shah, S., American Concrete Institute, Detroit, pp. 47-69.

21. Raithby, K., Galloway, J. (1974), "Effects of Moisture Condition, Age, and Rate of Loading on Fatigue of Plain Concrete", *Fatigue of Concrete*, American Concrete Institute, Detroit, pp. 15-34.

22. Klaiber, F., Lee, D. (1982), "The Effects of Air Content, Water-Cement Ratio, and Aggregate Type on the Flexural Strength of Plain Concrete", *Fatigue of Concrete Structures*, ed. Shah, S., American Concrete Institute, Detroit, pp. 111-131.

23. RILEM – Report of the Technical Committee 90-FMA Fracture Mechanics to Concrete – Applications (1989), *Fracture Mechanics of Concrete Structures*, edited by Elfgren, L., Chapman and Hall, New York.

24. Jenq, Y., Shah, S. (1985), " Two-Parameter Fracture model for Concrete", *Journal of Engineering Mechanics*, ASCE, Vol. 111, No. 10, 1985, pp. 1227-1241.

25. Nallathambi, P., Karihaloo, B. (1984), "Effect of specimen and crack size, water/cement ratio and coarse aggregate texture upon fracture toughness of concrete, *Mag Concr Res*, 15, pp.117-121.

26. Baluch, M., Qureshy, A., Azad, A. (1989), "Fatigue Crack Propagation in Plain Concrete", *Fracture of Concrete and Rock*, ed by Shah, S. et al., Springer-Verlag, New York, pp. 80-87.

27. Perdikaris, P., Calomino, A. (1989), "Kinetics of Crack Growth in Plain Concrete", *Fracture of Concrete and Rock*, ed by Shah, S. et al., Springer-Verlag, New York, pp. 64-69.

28. Chajes, M., Thomson, T., Januszka, T., Finch, W. (1994), "Flexural Strengthening of Concrete Beams Using Externally Bonded Composite Materials", *Construction and Building Materials*, 8(3), pp. 191-201.

29. Rotasy, R., Hankers, C., Ranisch, E. (1992), "Strengthening of Reinforced Concrete and Precast Concrete Structures with Bonded FRP Plates", *Advanced Composite Materials in Bridges and Structures*, Canadian Society for Civil Engineering.

30. Sierakowsi, R., Ross, C., Tedesco, J., Hughes, M. (1994), "Concrete Beams with Externally Bonded CFRP Strips", Proceedings of the Third Materials Engineering Conference, Infrastructure: New Materials and Methods of Repair, ASCE, San Diego, pp. 139-146.

31. Karbhari, V., Engineer, M. (1995), "On the Use of a Modified Peel Test for Determination of Concrete-Composite Bond Durability", 40th International SAMPE Symposium and Exhibition for the Society for the Advancement of material and Process Engineering, 40(2), pp. 1958-1970.

32. Xie, M., Karbhari, V. (1995), "Evaluation of Fracture Parameters in a Peel Test Specimen Using Finite Element Method", 40th International SAMPE

Symposium and Exhibition for the Society for the Advancement of material and Process Engineering, 40(2), pp. 1944-1957.

33. Drory, M., et al. (1987), "On the Decohesion of Residually Stressed Thin Films", *Acta Metall*, 36(8), pp. 2019-2028.

34. Buyukozturk, O., Hearing, B. (1997), "Failure Investigation of Concrete Beams Retrofitted with FRP Laminate", *Recent Advances in Bridge Engineering*, ed. Meier, U. and Betti, R., EMPA, Dubendorf, pp. 105-112.

35. Karihaloo, B. (1995), *Fracture Mechanics & Structural Concrete*, Longman Scientific & Technical, Essex, England.

36. Bazant, Z., Pfeiffer, P. (1985), "Test of Shear Fracture and Strain Softening in Concrete", 2nd Symposium on the Interaction of Non-Nuclear Munitions on Structures, Panama City Beach, FL.

APPENDIX

A.1 Static Loading Testing Data

Beam	FRP	Surface	Delam Locat. (In)	Dlm Load 1 (kips)	Dlm Mode 1	Dlm Load 2 (kips)	Dlm Mode 2
1	GFRP	Snddst	6	9.85	DLM	INC	DBD
2	GFRP	Snddst	9	9.88	DLF	9.01	DLS
3	GFRP	Snddst	12	9.03	DBD	9.63	DBD
4 ·	GFRP	Snddst	14	9.18	DLM	9.39	DLF
5	GFRP	Snddst	14	9.52	DLF	INC	DLS
6	GFRP	Smooth	6	8.25	DLM	9.09	DLS
7	GFRP	Smooth	9	7.57	DLM	9.03	DLM
8	GFRP	Smooth	9	8.43	DLM	NONE	NONE
9	GFRP	Smooth	12	7.89	DLM	7.90	DLF
10	GFRP	Smooth	12	7.99	DLM	NONE	NONE
11	GFRP	Smooth	12	8.29	DBD	INC	DLF
12	GFRP	Smooth	14	8.17	DBD	NONE	NONE
13	CFRP	Snddst	6	10.33	DLM	INC	DLS
14	CFRP	Snddst	6	10.30	DLM	INC	DBD
15	CFRP	Snddst	9	10.10	DLF	INC	DBD
16	CFRP ·	Snddst	10	9.92	DBD	9.62	DLF
17	CFRP	Snddst	10	9.99	DLM	INC	DLM
18	CFRP	Snddst	11	9.10	DBD	INC	DLS
19	CFRP	Snddst	12	9.75	DBD	8.31	DBD
20	CFRP	Snddst	14	9.82	DBD	INC	DLF
21	CFRP	Snddst	14	9.91	DLM	7.36	DLM
22	CFRP	Smooth	6	9.90	DBD	INC	DLF
23	CFRP	Smooth	9	9.42	DLS	9.29	DLM
24	CFRP	Smooth	12	8.90	DBD	INC	DLF
25	CFRP	Smooth	14	9.01	DLF	NONE	NONE

Table A.1: FRP Retrofitted Beams Tested under Static Loading

NONE – No delamination

INC- Inconclusive data to determine delamination load

Delamination loads and delamination modes are given for both ends of the beam. As shown in the table, some delamination loads were indiscernible as a gradual delamination of the concrete-laminate interface occurred. In these cases, the data was excluded. 'NONE' indicates that one side of the beam did not undergo laminate peel-off.

A.2 Cyclic Load Testing Data

data file	Side (L/R)	cycles	a init (in)	a fin (in)	max P (kips)	Pf init (kips)	Pf final (kips)	Pf ave (kips)	Pmx/Pf	da/dN (in/cyc)
B616	R	2100	4.5	6.9	7.5	10.78	10.27	10.53	0.71	1.1E-03
B616	L	2100	3.5	6.0	7.5	11.00	10.46	10.73	0.70	1.2E-03
B617	R	1200	7.9	8.7	6	10.06	9.88	9.97	0.60	6.8E-04
B617	L	1200	6.0	8.1	6	10.46	10.02	10.24	0.59	1.7E-03
B6111	R	1200	8.7	12.1	7.3	9.88	9.03	9.46	0.77	2.9E-03
B6111	L	1200	8.1	11.7	7.3	10.02	9.24	9.63	0.76	3.0E-03
B6112	R	1220	12.1	13.5	7	9.03	9.03	9.03	0.78	1.1E-03
B6112	L	1220	11.7	13.1	7	9.24	9.03	9.13	0.77	2.4E-03
B6127	L	1660	15.6	15.7	6.4	9.03	9.03	9.03	0.71	7.5E-05
B621	R	1200	3.0	3.3	6	11.11	11.05	11.08	0.54	2.1E-04
B625	R	1200	3.3	4.4	7.5	11.05	10.81	10.93	0.69	1.7E-03
B6211	R	900	5.6	5.9	6.5	10.54	10.49	10.52	0.62	2.8E-04
B6212	R	1200	5.9	6.4	6.5	10.49	10.38	10.44	0.62	4.2E-04
B6219	R	1200	6.4	8.9	6.8	10.38	9.84	10.11	0.67	2.1E-03
B6226	R	1200	8.9	13.6	8	9.84	9.03	9.44	0.85	4.5E-03
B6210	L	400	4.9	5.8	7.3	10.70	10.52	10.61	0.69	2.2E-03
B6217	L	1310	7.0	7.9	6.5	10.25	10.06	10.15	0.64	6.7E-04
B6222	L	1200	7.9	9.6	7.5	10.06	9.68	9.87	0.76	2.1E-03
B6241	L	1200	12.0	12.5	6.5	9.17	9.03	9.10	0.71	4.2E-04

a) CFRP Retrofitted Sandblasted Beams Tested under Cyclic Loading

data file	Side (L/R)	cycles	a init (in)	a fin (in)	max P (kips)	Pf init (kips)	Pf final (kips)	Pf ave (kips)	Pmx/Pf	da/dN (in/cyc)
B812	R	1200	3.0	3.2	6.5	10.39	10.36	10.37	0.63	1.6E-04
B8112	R	600	4.4	5.3	6.5	10.15	10.01	10.08	0.64	1.5E-03
B8120	R	1200	6.1	7.8	6.5	9.87	9.60	9.73	0.67	1.4E-03
B8123	R	1200	7.8	9.9	7.9	9.60	9.24	9.42	0.84	2.2E-03
B813	L	1200	3.0	3.7	7	10.39	10.28	10.33	0.68	8.3E-04
B818	L	1200	3.7	6.8	8.4	10.28	9.76	10.02	0.84	3.2E-03
B8110	L	1000	6.8	8.9	7.9	9.76	9.40	9.58	0.82	2.2E-03
B8117	L	1200	10.3	12.8	8	9.18	8.96	9.07	0.88	2.6E-03
B8131	R	1200	10.9	11.2	6.3	9.07	9.03	9.05	0.70	7.3E-04
B8132	R	800	11.2	11.9	6.8	9.03	8.90	8.96	0.76	9.4E-04
B8141	R	1200	12.5	13.0	6.3	8.96	8.96	8.96	0.70	4.2E-04
B8142	R	1200	13.0	13.3	6.8	8.96	8.96	8.96	0.76	2.1E-04
B8143	R	1200	13.3	13.4	7.3	8.96	8.96	8.96	0.81	1.6E-04
B71A1	R	1000	5.5	9.5	8	9.97	9.31	9.64	0.83	4.0E-03
B71A22	R	1200	15.8	16.5	6.8	8.96	8.96	8.96	0.76	6.3E-04
B71A1	L	1000	3.5	15.3	8	10.31	8.96	9.63	0.83	1.2E-02
B71A8	L	1200	12.0	13.1	7	8.89	8.96	8.92	0.78	9.4E-04

b) CFRP Retrofitted Smooth Beams Tested under Cyclic Loading

Table A.2: CFRP Retrofitted Beams Tested under Cyclic Loading